

A new transport model for flowing suspensions of active Brownian particles

Lloyd Fung¹†, Rachel N. Bearon² and Yongyun Hwang¹

¹Department of Aeronautics, Imperial College London, London SW7 2AZ, UK

²Department of Mathematical Sciences, University of Liverpool, Liverpool L69 7ZL, UK

(Received xx; revised xx; accepted xx)

A dilute suspension of motile micro-organisms subjected to a strong ambient flow, such as algae in the ocean, can be modelled as a population of non-interacting, orientable active Brownian particles (ABPs). Using the Smoluchowski equation (i.e. Fokker-Planck equation in space and orientation), one can capture the non-trivial transport phenomena of ABPs such as taxes and shear-induced migration. This work presents a method to transform the Smoluchowski equation into a physically-relevant transport equation analytically and an asymptotic approximation to the transformation. The approximation recovers the effective diffusivity given by the generalised Taylor dispersion (GTD) model in a quiescent flow as a dispersion tensor, but the approximation does not generate singularities in strain-dominant flows like the GTD model. The transformation has also unveiled the shear trapping mechanism previously shown by Bearon & Hazel (2015) and other new drift and dispersion mechanisms caused by the interactions between the orientational dynamics and the passive advection/diffusion of ABPs. Using gyrotactic suspensions in shear flow as an example, we show that the approximation is more accurate than the GTD model by accounting for shear trapping and the other new mechanisms for drift and dispersion. Lastly, we show that the dispersion from the translational diffusion can be negative, while the dispersion from the interaction between the rotational diffusion and the particles' motility can be highly asymmetric, in contrast to the positive definite effective diffusivity of the GTD model. The results open a new perspective on the nature and physical origin of the dispersion of ABPs in a general flow field.

1. Introduction

The transport of orientable micro-organisms or particles in a suspension is of fundamental importance for many ecological, medical and engineering applications. For example, the non-trivial macroscopic transport of motile species of phytoplankton is responsible for the formation of an ecological hotpot (Durham *et al.* 2009, 2013). The shape-dependent sedimentation of the non-motile species in turbulent water (Voth & Soldati 2017) may also be a significant factor affecting the carbon sequestration process in the ocean, a crucial process in the earth's carbon cycle. On the medical front, modelling the transport of bacteria helps us understand how they spread or propagate collectively on surfaces through swarming (see review by Koch & Subramanian 2011). In engineering, controlling the transport of bottom-heavy algal species in bioreactors may improve the harvesting of biofuel (Croze *et al.* 2013).

The macroscopic transport of particles is a key component in modelling the complex dynamics and rich collective behaviour of a suspension. While individual particles can be modelled with the Stokes equations given their small size (1-10 μm for bacteria and 10-100 μm for algae), the emergent behaviour or the flow environment is often at a larger length scale than the individuals (see review by Koch & Subramanian 2011; Elgeti *et al.* 2015; Clement *et al.* 2016; Bees 2020).

† Email address for correspondence: lloyd.fung12@imperial.ac.uk

The difference in length scale poses a significant challenge to the modelling of their collective behaviour.

Some of these emergent behaviours are the result of many-body interactions between particles. For example, bacterial turbulence and spontaneous self-organisation of bacterial suspension in confinement (Dombrowski *et al.* 2004; Wieland *et al.* 2013) are usually found in dense suspension where near-field hydrodynamic and/or steric interactions between particles are the driving mechanisms (Subramanian & Koch 2009; Saintillan & Shelley 2008, 2015; Lushi *et al.* 2014). In contrast, collective phenomena in dilute suspensions are usually the result of the non-trivial transport caused by some internal mechanisms of particles (e.g. 'taxes' for microorganisms) or sedimentation of orientable particles stemming from the flow-field-dependent orientation of individual particles. For example, bioconvection (see review by Bees 2020), unmixing (Durham *et al.* 2013) and gyrotactic shear trapping (Durham *et al.* 2009) are the result of the balancing influence of external fields (e.g. gravity, light or chemical gradient) and the flow field of the fluid on the particles' orientation. Other phenomena such as shear-trapping (Ezhilan & Saintillan 2015; Bearon & Hazel 2015; Vennamneni *et al.* 2020) and enhanced sedimentation (Clifton *et al.* 2018) are the results of the alignment of elongated particle with the flow field.

Microscopically, a Langevin equation is often used for the description of a particle's positional and rotational dynamics in the presence of thermal and/or biochemical noise. The typical approach to model the rotational dynamics of particles is to combine the Jeffery's Orbit (Jeffery 1922; Hinch & Leal 1972*a,b*), which governs how local vorticity and strain rate orient a particle, with other orientational biases responsible for the "taxes" such as gyrotaxis (Pedley & Kessler 1990), phototaxis (Drescher *et al.* 2010) and chemotaxis (Alt 1980). With the inclusion of a stochastic forcing arising from a variety of noise sources and additional suitable modelling of the interaction between particles (e.g. Batchelor 1970; Hinch & Leal 1972*a,b*; Pedley & Kessler 1990), one can perform simulations of many particles in the Stokes regime to capture some collective dynamics. However, there are several downsides to such individual-particle-based simulations. While these methods can capture some collective behaviours that involve hundreds or thousands of individual particles (e.g. Nott & Brady 1994; Brady & Morris 1997; Tornberg & Shelley 2004; Saintillan & Shelley 2007; Ishikawa *et al.* 2008; Delmotte *et al.* 2015; Schoeller & Keaveny 2018, etc.), it is expensive to scale up for phenomena involving several orders of magnitude more particles, given the computational cost for individual-based simulation. Furthermore, when the interactions between particles become important, the computational cost to resolve them increases even more quickly. Such a situation can be dealt with the Stokesian dynamics simulations (see Brady & Bossis 1988; Sierou & Brady 2001). However, this type of numerical tool is not applicable for large-scale fluid systems where inertial force is important in the dynamics (e.g. turbulence).

For such reasons, the present work instead employs the equation which describes the density distribution of the particles governed by the Langevin equation (Doi & Edwards 1988). Some (e.g. Saintillan (2018)) refer to the equation as the Fokker-Planck equation, but in this work, we shall refer to this equation as the Smoluchowski equation, so as not to be confused with the Fokker-Planck model introduced only for the particle orientation dynamics in early studies (Pedley & Kessler 1990, see also below). If the suspension is dilute, this "bottom-up" approach based on the Smoluchowski equation has some benefits over macroscopic phenomenological models proposed recently (e.g. Wensink *et al.* 2012; Dunkel *et al.* 2013; Słomka & Dunkel 2017). In particular, this approach directly incorporates the individual dynamics at microscale into the macroscopic continuum description, offering an explicit link between the micro- and macro-scale phenomena, although the description of near-field interactions between particles within this framework still remains an important challenge. Therefore, to simplify our work, we will limit the scope of the present study to the transport of particles in the dilute regime, where the long-range hydrodynamic contribution of particles can be modelled with the bulk stress tensors if

required (Pedley & Kessler 1990). While the dilute assumption may not be applicable to some of the aforementioned phenomena in dense suspension, it is justifiable in many phenomena in dilute suspensions, such as bioconvection and oceanographical phenomena, where the system size is large and the background flow is strong.

Despite the descriptive merit of the Smoluchowski-equation-based continuum model, there are only a handful of work that utilise a full numerical simulation of this equation (e.g. Chen & Jiang 1999; Saintillan & Shelley 2008; Saintillan 2010; Jiang & Chen 2020). This is due to the high number of dimensions in the equation, which makes it computationally too expensive. Past work overcame the challenge by taking a semi-heuristic approach to the transport of motile particles. In this type of approaches, the quasi-steady orientational distribution of particles under a certain flow field is solved separately, and the effective transport coefficients (i.e. advection velocity and diffusivity) are estimated using a phenomenological model, such as the Fokker-Planck (FP) model (Pedley & Kessler 1990; Pedley 2010) or the generalised Taylor dispersion (GTD) theory (Hill & Bees 2002; Bearon 2003; Manela & Frankel 2003). These models describe the particle's orientation dynamics only using the 'local' flow information, reducing the number of dimensions needed while keeping the effect of the flow field on the transport properties intact. Recent works such as Croze *et al.* (2013, 2017) and Fung *et al.* (2020) showed that the FP model of Pedley & Kessler (1990) is not as accurate as the GTD model at high shear rates. This is because the effective diffusion in the FP model is a phenomenological approximation with an *ad hoc* constant for unknown diffusion time scale, and is not based on the Smoluchowski equation like the GTD model. Despite this merit, the GTD model also has an important limitation – it is only applicable to vorticity-dominant flows due to the singularity in its effective diffusivity emerging in strain-rate-dominant flows (Bearon *et al.* 2011). Indeed, in a recent review (Bees 2020), this limitation of the GTD model has been pointed out as a significant challenge for the modelling of bioconvection. Moreover, the GTD model was derived for a homogenous shear flow. When applied to inhomogeneous shear flow, it would then implicitly assume a quasi-homogeneous shear of the flow field. Therefore, it is not able to describe the extra advection (or drift) caused by the inhomogeneity in flow shear, and fails to capture the related phenomena such as the shear trapping of non-biased motile particles (Bearon & Hazel 2015; Veniamneni *et al.* 2020).

This work aims to propose a new transport model for the orientable particles to overcome the inherent limitations of the GTD model and the inaccuracy of the Fokker-Planck model. We will show that the Smoluchowski equation admits an exact transformation into a transport equation which share many similarities to the platform used in the FP model and the GTD model. Combining this transformation with the method of multiple scales, this work proposes a novel transport equation, in which the orientation dynamics is determined only with the local flow information in the physical space like the FP and the GTD model. We will show that this new model not only removes the limitations of the GTD model, but it also offers more accurate predictions for the active particle distribution in inhomogeneous shear flow.

This work is organised as follow. In §2, the Smoluchowski is presented with the equations governing the motion of active (or swimming) Brownian particles. We will also briefly introduce the GTD model and its inherent restriction. In §3, the exact transformation of the Smoluchowski equation into a transport equation is introduced. While the transformed equation cannot be directly used as a model, it sets up the mathematical platform for the further local approximation presented in §4. In §4, the local approximation is presented for the development of novel transport equation model, and the mathematical structure of this model is compared with that of the GTD model. In §5, we present examples of gyrotactic particle suspensions in one-dimensional vertical and horizontal shear flows, and demonstrate the superiority of the newly-introduced model over the GTD model. We will also compare these results with those obtained through the exact transformation of the Smoluchowski equations. In §6, we further dissect the physical implication of the transformation in comparison to the GTD model, and discuss the physical origin of the

dispersion of particles. Lastly, in §7, we will briefly outline the potential application of the local approximation and the challenges remains with the proposed model.

2. Background

2.1. The Smoluchowski equation

We consider a dilute suspension of active Brownian particles (ABPs), and the randomness in their motion is present in the physical space \mathbf{x}^* and orientational space \mathbf{p} . In this study, the term ABP will be used to refer to a self-propelling particle (or microswimmer) subject to a translational and/or rotational random walk. Given the stochastic nature of the trajectory, we consider the number density distribution function $\Psi(\mathbf{x}^*, \mathbf{p}, t^*)$ for particles located at \mathbf{x}^* with orientation \mathbf{p} at time t^* . The equation for $\Psi(\mathbf{x}^*, \mathbf{p}, t^*)$ is governed by the Smoluchowski equation (Doi & Edwards 1988)

$$\frac{\partial \Psi}{\partial t^*} + \nabla_{\mathbf{x}}^* \cdot [\dot{\mathbf{x}}^* \Psi - D_T^* \nabla_{\mathbf{x}}^* \Psi] + \nabla_{\mathbf{p}} \cdot [\dot{\mathbf{p}}^* \Psi - d_r^* \nabla_{\mathbf{p}} \Psi] = 0, \quad (2.1)$$

where the deterministic motion for $\dot{\mathbf{x}}^*$ is governed by

$$\dot{\mathbf{x}}^* = \mathbf{u}^* + V_c^* \mathbf{p}. \quad (2.2)$$

Here, the superscript $(\cdot)^*$ represents dimensional variables or parameters, \mathbf{u}^* is the prescribed flow velocity and $V_c^* \mathbf{p}$ the velocity of particles by the active motion (swimming / motility). Meanwhile, the deterministic form of orientational dynamics for $\dot{\mathbf{p}}^*$ is governed by

$$\dot{\mathbf{p}}^* = \left(\frac{\Omega^*(\mathbf{x})}{2} \wedge \mathbf{p} + \alpha_0 \mathbf{p} \cdot \mathbf{E}^* \cdot (\mathbf{I} - \mathbf{p}\mathbf{p}) \right) + \frac{1}{2B^*} [\mathbf{k} - (\mathbf{k} \cdot \mathbf{p})\mathbf{p}]. \quad (2.3)$$

Here, we assume that the particle is oriented by the local flow through the Jeffery's equation (Jeffery 1922; Bretherton 1962), where $\Omega^* = \nabla_{\mathbf{x}}^* \wedge \mathbf{u}^*$ is the vorticity, $\mathbf{E}^* = (\nabla_{\mathbf{x}}^* \mathbf{u}^* + \nabla_{\mathbf{x}}^* \mathbf{u}^{*T})/2$ the rate-of-strain tensor and α_0 the Bretherton constant. In this work, we also consider gyrotaxis of the given particles (Pedley & Kessler 1990), as will be used for the flow examples in §5. This is the second term in the right-hand side of (2.3) where \mathbf{k} is the unit vector pointing upwards (against gravity) and B^* the gyrotactic time scale.

In (2.1), we have also assumed that the random motions in \mathbf{x} - and \mathbf{p} -space can be modelled as translational diffusion with the corresponding diffusivity D_T^* and rotational diffusion with the diffusivity d_r^* , respectively. The translational diffusion D_T^* often originates from thermal fluctuation especially for small particles. However, it is often negligible for many micro-organisms (e.g. microalgae), given their relatively large size. In this study, we will keep this term without loss of generality, so that proposed framework can be extended to other types of particles.

Equation (2.1) is subsequently non-dimensionalised with suitable length and time scales. In this work, the characteristic length h^* was chosen from the given flow field, and the inverse of rotational diffusivity $1/d_r^*$ was chosen for the time scale. For convenience, we shall also use the characteristic speed U^* of the flow for the non-dimensionalisation. Hence,

$$\mathbf{x} = \frac{\mathbf{x}^*}{h^*}, \quad t = t^* d_r^*, \text{ and} \quad \mathbf{u} = \frac{\mathbf{u}^*}{U^*},$$

and the dimensionless parameters for the speed of motility (swimming) V_s^* , the flow speed U^* , the translational diffusivity D_T^* and the gyrotactic timescale B^* , and their equivalent non-dimensionalised parameters are

$$Pe_s = \frac{V_s^*}{h^* d_r^*}, \quad Pe_f = \frac{U^*}{h^* d_r^*}, \quad D_T = \frac{D_T^*}{(h^*)^2 d_r^*}, \quad \text{and} \quad \beta = \frac{1}{2d_r^* B^*},$$

respectively, where Pe_f and Pe_s are the ambient flow and motility Péclet numbers. The dimensionless form of (2.1) is then given by

$$\frac{\partial \Psi}{\partial t} + \nabla_{\mathbf{x}} \cdot [(Pe_f \mathbf{u} + Pe_s \mathbf{p}) \Psi] + \mathcal{L}_p(\mathbf{x}, t) \Psi = D_T \nabla_{\mathbf{x}}^2 \Psi, \quad (2.4)$$

where we also introduce the \mathbf{p} -space linear operator

$$\mathcal{L}_p(\mathbf{x}, t) \Psi = \nabla_{\mathbf{p}} \cdot \left[\left(\frac{Pe_f}{2} \boldsymbol{\Omega} \wedge \mathbf{p} + Pe_f \alpha_0 \mathbf{p} \cdot \boldsymbol{E} \cdot (\mathbf{I} - \mathbf{p}\mathbf{p}) + \beta [\mathbf{k} - (\mathbf{k} \cdot \mathbf{p})\mathbf{p}] \right) \Psi \right] - \nabla_{\mathbf{p}}^2 \Psi \quad (2.5)$$

Therefore, by the divergence theorem, the integration over \mathbf{p} -space of the operator $\mathcal{L}_p(\mathbf{x}, t)$ acting on any arbitrary function $a(\mathbf{p})$ satisfies

$$\int_{S_p} \mathcal{L}_p(\mathbf{x}, t) a(\mathbf{p}) d^2 \mathbf{p} = 0, \quad (2.6)$$

where S_p is the unit sphere, i.e. the \mathbf{p} -space subject to $\|\mathbf{p}\| = 1$. Physically, it is related to the conservation of probability distribution in \mathbf{p} -space. We also note that (2.5) may be modified to account for other taxes by including the relevant modelling terms: e.g. the run-and-tumble and chemotaxis process (Subramanian & Koch 2009) or phototaxis (Williams & Bees 2011). Therefore, we expect that many deterministic models for the orientation dynamics in \mathbf{p} -space would be given as a linear operator $\mathcal{L}_p(\mathbf{x})$ that satisfies (2.6). Without loss of generality, in the following sections, we will use the linear operator $\mathcal{L}_p(\mathbf{x}, t)$ to represent the orientation dynamics in \mathbf{p} -space.

2.2. The generalised Taylor dispersion model

The GTD model was originally derived by Brenner (1980), and later extended by Frankel & Brenner (1989, 1991, 1993). It is a theoretical framework which approximates the particle transport governed by (2.1) into an advection-diffusion equation. Recent studies (Croze *et al.* 2013, 2017) have shown that it offers a more accurate and physically relevant description for active particle transport both in stationary and sheared suspensions (see Saintillan 2018; Fung *et al.* 2020; Bees 2020). However, its application has so far been limited to unidirectional shear flow (Bearon *et al.* 2011) due to the difficulties discussed in §1. In this subsection, we will also give a brief overview of the theory and how the limitation arises.

To start with, the GTD model is based on two assumptions: 1) the timescale in \mathbf{p} -space is much faster than that of \mathbf{x} -space (quasi-steady assumption); 2) the size of the particle is much smaller than the length scale of the flow, allowing to set velocity gradient tensor $\nabla \mathbf{u}$ to be locally constant (quasi-uniform shear assumption). Under these assumptions, the GTD model obtains the effective drift and diffusivity using the impulse response of (2.4), which describes the probability density function of a single particle in terms of \mathbf{p} and \mathbf{x} . Then the solution to (2.4) is utilised to approximate the effective drift and diffusivity using their definitions given in terms of the Oldroyd time derivative of first and second statistical moments in the limit of $t \rightarrow \infty$ (for further details, see Frankel & Brenner 1991, 1993). The resulting advection-diffusion (or drift-diffusion) equation for the particle distribution $n(\mathbf{x}, t)$ is given by (Manela & Frankel 2003; Hill & Bees 2002)

$$\partial_t n + \nabla_{\mathbf{x}} \cdot [(Pe_s \langle \mathbf{p} \rangle_g + Pe_f \mathbf{u}) n] = D_T \nabla_{\mathbf{x}}^2 n + Pe_s^2 \nabla_{\mathbf{x}} \cdot \mathbf{D}_{GTD} \nabla_{\mathbf{x}} n, \quad (2.7a)$$

where

$$\langle \mathbf{p} \rangle_g(\mathbf{x}, t) \equiv \int_{S_p} \mathbf{p} g(\mathbf{x}, t; \mathbf{p}) d^2 \mathbf{p}, \quad (2.7b)$$

with

$$\mathcal{L}_p(\mathbf{x}, t)g(\mathbf{x}, t; \mathbf{p}) = 0 \quad \text{subject to} \quad (2.7ca)$$

$$\int_{S_p} g(\mathbf{x}, t; \mathbf{p}) d^2 \mathbf{p} = 1, \quad (2.7cb)$$

Meanwhile, the effective diffusivity \mathbf{D}_{GTD} is computed by

$$\mathcal{L}_p \mathbf{b}_{GTD} - Pe_f \mathbf{b}_{GTD} \cdot \mathbf{G} = (\mathbf{p} - \langle \mathbf{p} \rangle_g) g, \quad (2.7d)$$

leading to

$$\mathbf{D}_{GTD} = \int_{S_p} \left[\mathbf{b}_{GTD} \mathbf{p} + Pe_f \frac{\mathbf{b}_{GTD} \mathbf{b}_{GTD} \cdot \mathbf{G}}{g} \right]^{sym} d^2 \mathbf{p}. \quad (2.7e)$$

where $\mathbf{G} = \nabla \mathbf{u}$ is the velocity gradient tensor. Here, note that the advective drift caused by the particles' motility is obtained from the ensemble-averaged velocity of individual particles, given that its orientational distribution is $g(\mathbf{x}, t; \mathbf{p})$. The term $Pe_s \langle \mathbf{p} \rangle_g$ can therefore be interpreted as the average motility of individual particles. Furthermore, symmetry is enforced to the tensor \mathbf{D}_{GTD} in (2.7e), given its definition based on the second-order statistical moment of the ensemble-averaged particle spatial displacement.

As mentioned earlier, the GTD model has an important limitation in applications to general shear flows in which various forms of \mathbf{G} would appear. The formulae (2.7d) and (2.7e) proposed in Frankel & Brenner (1991, 1993) were derived by extending the original GTD theory in a quiescent flow (Frankel & Brenner 1989) to a homogeneous shear flow. For this purpose, Frankel & Brenner (1991) introduced a transformation which maps the position in a sheared suspension into that in a stationary one, such that the original theoretical framework in Frankel & Brenner (1989) can be applied. The transformation resulted in the extra terms $-\mathbf{b}_{GTD} \cdot \mathbf{G}$ and $\mathbf{b}_{GTD} \mathbf{b}_{GTD} \cdot \mathbf{G}/g$ in (2.7d) and (2.7e). In principle, the mapping is only valid if $\text{Re}(\text{eig}(\mathbf{G})) \leq 0$, thereby restricting the framework's applicability to the subset of shear flows which are not strain-dominated. Moreover, if $\text{Re}(\text{eig}(\mathbf{G})) > 0$, the left-hand-side operator on \mathbf{b}_{GTD} in (2.7d) might become singular, resulting in singular \mathbf{b}_{GTD} and \mathbf{D}_{GTD} . For example, Bearon *et al.* (2011) demonstrated the singularity in \mathbf{D}_{GTD} as a function of local velocity gradient \mathbf{G} in straining-dominated region of a two dimensional convective cell.

3. Exact transformation into a transport equation

The purpose of this work is to obtain a transport equation which resembles the GTD model (2.7) proposed by Frankel & Brenner (1991, 1993). The key approach taken by Frankel & Brenner (1991, 1993) lies in the approximation of the Oldroyd time derivative of the first- and second-order statistical moments using Ψ in (2.4) for the "phenomenological" effective drift $Pe_s \langle \mathbf{p} \rangle$ and diffusivity \mathbf{D}_{GTD} . Instead, in this work, we shall start by seeking an exact mathematical transformation of (2.4) into such a transport equation which resembles (2.7) of the GTD model. In particular, this transformation will be utilised in §4 as the foundation for a novel transport-equation-based model, which overcomes the limitations of the GTD model.

We define $n(\mathbf{x}, t)$ and $f(\mathbf{x}, \mathbf{p}, t)$ as $\Psi(\mathbf{x}, \mathbf{p}, t) = n(\mathbf{x}, t)f(\mathbf{x}, \mathbf{p}, t)$, so that $f(\mathbf{x}, \mathbf{p}, t)$ at each \mathbf{x} becomes the probability density function in \mathbf{p} space satisfying $\int_{S_p} f(\mathbf{p}) d^2 \mathbf{p} = 1$. Now, from (2.6), integration of (2.4) over \mathbf{p} -space gives the following equation in the (\mathbf{x}, t) space,

$$\partial_t n(\mathbf{x}, t) + \nabla_{\mathbf{x}} \cdot [(Pe_s \langle \mathbf{p} \rangle_f(\mathbf{x}, t) + Pe_f \mathbf{u}(\mathbf{x}, t))n(\mathbf{x}, t)] = D_T \nabla_{\mathbf{x}}^2 n(\mathbf{x}, t), \quad (3.1)$$

where

$$\langle \mathbf{p} \rangle_f(\mathbf{x}, t) \equiv \int_{S_p} \mathbf{p} f(\mathbf{x}, \mathbf{p}, t) d^2 \mathbf{p}. \quad (3.2)$$

| Terms | Physical meaning |
|--|---|
| $n \partial_t f$ | Unsteadiness of f in \mathbf{p} -space |
| $Pe_f n \mathbf{u} \cdot \nabla_{\mathbf{x}} f$ | Passive advection of f in \mathbf{x} by the ambient flow \mathbf{u} |
| $-D_T (\nabla_{\mathbf{x}}^2 f) n$ | Translational diffusion of f in \mathbf{x} |
| $-2D_T (\nabla_{\mathbf{x}} f) \cdot (\nabla_{\mathbf{x}} n)$ | Cross-translation diffusion in \mathbf{x} between n and f |
| $Pe_s (\mathbf{p} f - \langle \mathbf{p} \rangle_f f) \cdot \nabla_{\mathbf{x}} n$ | Change in f induced by motility and gradient of particle distribution in \mathbf{x} |
| $Pe_s n (\mathbf{p} \cdot \nabla_{\mathbf{x}} f - f \nabla_{\mathbf{x}} \cdot \langle \mathbf{p} \rangle_f)$ | Change in f induced by motility and inhomogeneity of f in \mathbf{x} |

Table 1: Physical meaning of each term in equation (3.3)

Here, we note that (3.1) appears as a standard advection-diffusion equation. However, in the absence of the full information of $\Psi(\mathbf{x}, \mathbf{p}, t)$, it is not solvable because $\langle \mathbf{p} \rangle_f(\mathbf{x}, t)$ is still unknown. Furthermore, the precise physical implication of the drift term $Pe_s \langle \mathbf{p} \rangle_f(\mathbf{x}, t)$ remains not clear, especially compared to the particle drift $Pe_s \langle \mathbf{p} \rangle_g$ in (2.7a) (Frankel & Brenner 1991, 1993; Hill & Bees 2002; Manela & Frankel 2003). Therefore, it would be useful if there is an alternative form of (3.1), in which $\langle \mathbf{p} \rangle_f(\mathbf{x}, t)$ can be replaced with $\langle \mathbf{p} \rangle_g(\mathbf{x}, t)$ and the other related terms. More discussion on the comparison between $\langle \mathbf{p} \rangle_f$ and $\langle \mathbf{p} \rangle_g$ will follow in §6.1.

Multiplying (3.1) by $f(\mathbf{x}, \mathbf{p}, t)$ and subtracting it from (2.4) give

$$\begin{aligned} n \partial_t f + (Pe_f \mathbf{u} \cdot \nabla_{\mathbf{x}} f - D_T \nabla_{\mathbf{x}}^2 f) n - 2D_T (\nabla_{\mathbf{x}} f) \cdot (\nabla_{\mathbf{x}} n) \\ + Pe_s (\mathbf{p} f - \langle \mathbf{p} \rangle_f f) \cdot \nabla_{\mathbf{x}} n + Pe_s n (\mathbf{p} \cdot \nabla_{\mathbf{x}} f - f \nabla_{\mathbf{x}} \cdot \langle \mathbf{p} \rangle_f) \\ + n \mathcal{L}_p(\mathbf{x}, t) f = 0, \end{aligned} \quad (3.3)$$

each term of which may be interpreted physically as described in Table 1. Next, we introduce the following set of linear equations which use each term in (3.5) as the driving term:

$$\mathcal{L}_p(\mathbf{x}, t) f_u(\mathbf{x}, \mathbf{p}, t) = Pe_f \mathbf{u} \cdot \nabla_{\mathbf{x}} f, \quad (3.4a)$$

$$\mathcal{L}_p(\mathbf{x}, t) f_{D_T}(\mathbf{x}, \mathbf{p}, t) = -D_T \nabla_{\mathbf{x}}^2 f, \quad (3.4b)$$

$$\mathcal{L}_p(\mathbf{x}, t) \mathbf{b}_{D_T}(\mathbf{x}, \mathbf{p}, t) = -2D_T \nabla_{\mathbf{x}} f, \quad (3.4c)$$

$$\mathcal{L}_p(\mathbf{x}, t) \mathbf{b}_c(\mathbf{x}, \mathbf{p}, t) = Pe_s (\mathbf{p} - \langle \mathbf{p} \rangle_f) f, \quad (3.4d)$$

$$\mathcal{L}_p(\mathbf{x}, t) f_c(\mathbf{x}, \mathbf{p}, t) = Pe_s (\mathbf{p} \cdot \nabla_{\mathbf{x}} f - f \nabla_{\mathbf{x}} \cdot \langle \mathbf{p} \rangle_f), \quad (3.4e)$$

$$\mathcal{L}_p(\mathbf{x}, t) f_{\partial t}(\mathbf{x}, \mathbf{p}, t) = \partial_t f. \quad (3.4f)$$

Here, the solutions f_{\star} and \mathbf{b}_{\star} , with $(\cdot)_{\star}$ indicating any subscript above, are subjected to the integral condition $\int_{S_p} f_{\star} d^2 \mathbf{p} = 0$ or $\int_{S_p} \mathbf{b}_{\star} d^2 \mathbf{p} = \mathbf{0}$, so as not to contain the homogeneous solution. This enables us to uniquely define the solutions to (3.4). Also, given (2.6), (3.4) is valid if integration of the right-hand-side of each of (3.4) over \mathbf{p} -space is zero, and this is ensured by the form of (3.3). Lastly, we note that the introduced variables are still functions of both \mathbf{x} and t , because \mathcal{L}_p can have coefficients varying in \mathbf{x} and f depends on both \mathbf{x} and t . With the introduced variables, (3.3) can be rewritten as

$$[\mathcal{L}_p(\mathbf{b}_{D_T} + \mathbf{b}_c)] \cdot \nabla_{\mathbf{x}} n + [\mathcal{L}_p(f_u + f_{D_T} + f_c + f_{\partial t} + f)] n = 0. \quad (3.5)$$

This leads to

$$[\mathbf{b}_{D_T} + \mathbf{b}_c] \cdot \nabla_{\mathbf{x}} n + [f_u + f_{D_T} + f_c + f_{\partial t} + f] n = n g, \quad (3.6)$$

Terms Physical meaning

| | |
|--------------------------------|---|
| $\langle \mathbf{p} \rangle_g$ | Averaged motility of individual particle from the homogeneous solution of \mathcal{L}_p |
| $\mathbf{V}_{\partial t}$ | Drift due to interaction between particles' orientational dynamics and the unsteadiness of f in \mathbf{p} -space |
| \mathbf{V}_u | Drift due to interaction between particles' orientational dynamics and passive advection of f in \mathbf{x} by the flow field \mathbf{u} |
| \mathbf{V}_c | Drift due to interaction between particles' motility and the inhomogeneity of particles' orientational dynamics in \mathbf{x} |
| \mathbf{V}_{D_T} | Drift due to interaction between particles' orientational dynamics and translational diffusion of f in \mathbf{x} |
| \mathbf{D}_{D_T} | Dispersion from interaction between particles' orientational dynamics and the dispersion of n and f due to translational diffusion of f and n |
| \mathbf{D}_c | Dispersion due to interaction between particles' motility and orientational dynamics |

Table 2: Physical meaning of each derived term in equation (3.11)

where the homogeneous solution $g(\mathbf{x}, t; \mathbf{p})$, defined by

$$\mathcal{L}_p(\mathbf{x}, t)g(\mathbf{x}, t; \mathbf{p}) = 0 \quad \text{subject to} \quad (3.7a)$$

$$\int_{S_p} g(\mathbf{x}, t; \mathbf{p}) d^2 \mathbf{p} = 1, \quad (3.7b)$$

is added with n which can be obtained by integrating (3.6) over \mathbf{p} space.

Note that (3.6) is merely a different form of (3.3). Multiplying \mathbf{p} by (3.6) and integrating in \mathbf{p} -space then yield

$$(\mathbf{D}_{D_T} + \mathbf{D}_c) \cdot \nabla_{\mathbf{x}} n + [\mathbf{V}_u + \mathbf{V}_{D_T} + \mathbf{V}_c + \mathbf{V}_{\partial t} + \langle \mathbf{p} \rangle_f] n = n \langle \mathbf{p} \rangle_g, \quad (3.8)$$

where

$$\mathbf{V}_\star(\mathbf{x}, t) = \int_{S_p} \mathbf{p} f_\star(\mathbf{x}, \mathbf{p}, t) d^2 \mathbf{p}, \quad (3.9)$$

$$\mathbf{D}_\star(\mathbf{x}, t) = \int_{S_p} \mathbf{p} \mathbf{b}_\star(\mathbf{x}, \mathbf{p}, t) d^2 \mathbf{p} \quad (3.10)$$

with $(\cdot)_\star$ indicating any of the subscripts used in (3.4).

Now, replacing $n \langle \mathbf{p} \rangle_f$ in (3.1) with that of (3.8) leads to the following transport equation:

$$\begin{aligned} \partial_t n + \nabla_{\mathbf{x}} \cdot [(&P_{ef} \mathbf{u} + P_{es} (\langle \mathbf{p} \rangle_g - \mathbf{V}_u - \mathbf{V}_{D_T} - \mathbf{V}_c - \mathbf{V}_{\partial t})) n] \\ = D_T \nabla_{\mathbf{x}}^2 n + P_{es} \nabla_{\mathbf{x}} \cdot (\mathbf{D}_{D_T} + \mathbf{D}_c) \cdot \nabla_{\mathbf{x}} n. \end{aligned} \quad (3.11)$$

The important benefit of (3.11) is that it has the mathematical structure comparable to (2.7a) of the GTD model, as they share $P_{es} \langle \mathbf{p} \rangle_g$ representing the average motility of individual particles. Furthermore, this is an exact transport equation directly obtained from (2.4) without making any assumptions. However, it should be mentioned that (3.11) is not the only transport equation one can obtain from (2.4) – indeed, we already have retrieved a different form of a transport equation (3.1) from (2.4). This is essentially the consequence of reducing the dimensions of the given system (2.4) from the (\mathbf{x}, \mathbf{p}) -space to just \mathbf{x} -space. In fact, the step from (3.6) to (3.8) implies that there can be as many versions of (3.8) as one can make a different choice for the vector in place of \mathbf{p} (i.e. infinitely many). These arbitrary equations can then be summed with (3.1) to get some transport equations. However, the particular choice \mathbf{p} as the multiplication factor for this step is

probably the most physically relevant because the resulting expression in (3.8) decomposes $\langle \mathbf{p} \rangle_f$ in (3.1) into the averaged motility of individual particle $Pe_s \langle \mathbf{p} \rangle_g$ and the other terms from (2.4). Hence, each term in (3.11) would also admit physical implications, as listed in table 2. More importantly, later in §4.2, we will further show how $\langle \mathbf{p} \rangle_g$ and \mathbf{D}_c in (3.11) can be related to the effective drift and diffusivity in (2.7a) of the GTD model. Lastly, it is also important to note that \mathbf{D}_{D_T} and \mathbf{D}_c in (3.11) do not necessarily describe a diffusion process, as they are not guaranteed to be either symmetric or positive definite. Therefore, one should be careful in understanding their actual roles, and, in this sense, (3.11) cannot precisely be referred to as an advection-diffusion equation. More discussions on this issue will follow in §4.2 and §6.2.

4. A new transport equation model using local flow information

While the transport equation in (3.11) is obtained without making any assumption to (2.4), the formulae for \mathbf{V}_\star and \mathbf{D}_\star given in (3.4) are based on $f = \Psi/n$, requiring the full knowledge of Ψ (i.e. the solution to (2.4)). Therefore, the transformation discussed in §3 does not alleviate the difficulty related to the computational cost of the full Smouhowski equation (2.4). To resolve this issue, in this section, we will combine the transformation technique leading to (3.8) with a multiple time-scale asymptotic analysis. This results in an approximated form of (3.11) utilising only the local flow information (i.e. local approximation).

4.1. Local approximation of the transformed transport equation

First, we assume $Pe_s (\equiv \epsilon) \ll 1$, $Pe_f \lesssim O(\epsilon)$ and $D_T \lesssim O(\epsilon)$, and define $\tilde{Pe}_f = Pe_f/\epsilon$ and $\tilde{D}_T = D_T/\epsilon$. Physically, these assumptions imply that the timescale in the orientational \mathbf{p} -space is much faster than that in \mathbf{x} -space (i.e. quasi-steady assumption). Hence, the orientational component of Ψ (i.e. $f(\mathbf{x}, \mathbf{p}, t)$) will first relax to quasi-equilibrium in \mathbf{p} -space while the \mathbf{x} -dependency of Ψ is still evolving slowly. This then enables us to introduce a slowly-varying time scale $T = \epsilon t$ for the dynamics of Ψ in \mathbf{x} -space. The standard multiple-scale asymptotic analysis is subsequently applied by expanding $\Psi = \Psi^{(0)} + \epsilon\Psi^{(1)} + \epsilon^2\Psi^{(2)} + O(\epsilon^3)$. Following a similar transformation to that in §3 and retaining the terms up to $O(\epsilon^2)$ (see appendix A for further details), we derive an approximated transport equation given by

$$\begin{aligned} \partial_t n + \nabla_{\mathbf{x}} \cdot [Pe_s (\langle \mathbf{p} \rangle_g + \tilde{Pe}_f \mathbf{u}) n - Pe_s^2 (\mathbf{V}_{g,u} + \mathbf{V}_{g,D_T} + \mathbf{V}_{g,c} + \mathbf{V}_{g,\partial T}) n] \\ \approx Pe_s \tilde{D}_T \nabla_{\mathbf{x}}^2 n + Pe_s^2 \nabla_{\mathbf{x}} \cdot [(\mathbf{D}_{g,c} + \mathbf{D}_{g,D_T}) \nabla_{\mathbf{x}} n] \end{aligned} \quad (4.1)$$

for the transport of $n(\mathbf{x}, t)$, where the drifts and dispersion coefficients are defined by (3.9-3.10) and

$$\mathcal{L}_p(\mathbf{x}, T) f_{g,u}(\mathbf{x}, T; \mathbf{p}) = \tilde{Pe}_f \mathbf{u} \cdot \nabla_{\mathbf{x}} g, \quad (4.2a)$$

$$\mathcal{L}_p(\mathbf{x}, T) f_{g,D_T}(\mathbf{x}, T; \mathbf{p}) = -\tilde{D}_T \nabla_{\mathbf{x}}^2 g, \quad (4.2b)$$

$$\mathcal{L}_p(\mathbf{x}, T) \mathbf{b}_{g,D_T}(\mathbf{x}, T; \mathbf{p}) = -2\tilde{D}_T \nabla_{\mathbf{x}} g, \quad (4.2c)$$

$$\mathcal{L}_p(\mathbf{x}, T) \mathbf{b}_{g,c}(\mathbf{x}, T; \mathbf{p}) = (\mathbf{p} - \langle \mathbf{p} \rangle_g) g, \quad (4.2d)$$

$$\mathcal{L}_p(\mathbf{x}, T) f_{g,c}(\mathbf{x}, T; \mathbf{p}) = (\mathbf{p} \cdot \nabla_{\mathbf{x}} g - g \nabla_{\mathbf{x}} \cdot \langle \mathbf{p} \rangle_g). \quad (4.2e)$$

$$\mathcal{L}_p(\mathbf{x}, T) f_{g,\partial T}(\mathbf{x}, T; \mathbf{p}) = \partial_T g, \quad (4.2f)$$

where all $f_{g,\star}$ and $\mathbf{b}_{g,\star}$ are subjected to the integral condition $\int_{S_p} d^2 \mathbf{p} = 0$. The approximated transport equation (4.1) is identical to (3.11), except that their coefficients in (4.2) are now obtained by replacing f in (3.4) with g in (3.7a). This is a crucial advantage of (4.1) over (3.11) because g in (3.7a) can be solved pointwisely at each \mathbf{x} if the local flow information (i.e. $\mathbf{\Omega}$ and \mathbf{E}) is known. Therefore, (4.1) no longer requires the full solution to (2.4).

Here, the derivation above is similar to that of the shear trapping in Bearon & Hazel (2015) and

Vennamneni *et al.* (2020). However, in deriving (4.1), we have assumed $T = \epsilon t$. This time-scale separation is different from $T = \epsilon^2 t$ of Bearon & Hazel (2015) and Vennamneni *et al.* (2020). We note that $\mathbf{V}_{g,\star}$ and $\mathbf{D}_{g,\star}$ terms in (4.1) scale with Pe_s^2 , while the rest of the equation scales with Pe_s . Therefore, the effect of these terms appear only at $O(\epsilon^2)$, while the rest of the terms are still non-zero at $O(\epsilon)$. This is contrast to the flows considered in Bearon & Hazel (2015) and Vennamneni *et al.* (2020). In their cases, the translational diffusion was negligible ($D_T = 0$), the averaged orientation of individual particles was not biased ($\langle \mathbf{p} \rangle_g = \mathbf{0}$), and the flow was parallel such that $\mathbf{u} \cdot \nabla_{\mathbf{x}} = 0$. Hence, if $T = \epsilon t$ was assumed, the equation at $O(\epsilon)$ would simply lead to the trivial solution. However, in general, there is no reason that the leading-order equation has to have such a trivial solution especially in the presence of taxes, translational diffusion, or a non-parallel flow field. Therefore, these leading order effects require us to retain the scaling $T = \epsilon t$ in this work.

4.2. Comparison with the GTD model

The GTD model was derived semi-heuristically by evaluating an effective drift and diffusion coefficient using their definitions given in terms of the Oldroyd time derivative of first and second statistical moments of particle displacement (Frankel & Brenner 1991, 1993). In contrast, the local-approximation model in (4.1) was directly derived from the Smoluchowski equation (2.4). Despite the fundamentally different derivation procedures, (2.7a) of the GTD model and (4.1) of the local approximation model in this study share a lot in common. Apart from the same flow advection ($Pe_f \mathbf{u}$) and diffusion (D_T) terms, they share the same individual particles' motility $Pe_s \langle \mathbf{p} \rangle_g$ and have similar form of effective diffusivity \mathbf{D}_{GTD} and dispersion $\mathbf{D}_{g,c}$. In particular, the two models become identical for stationary non-diffusive ($Pe_f = D_T = 0$) suspensions, as will be shown below. These similarities suggest that the transformed equation (3.11) and its local approximation (4.1) are not only mathematically useful but also physically meaningful. In this subsection, we will make a detailed comparison between the GTD model and the local approximation model from a theoretical perspective. Further comparisons will follow in §5 with some flow examples.

(i) *Assumptions*: Both the GTD model and the local approximation model assume that the time scale in \mathbf{p} -space is much faster than that of \mathbf{x} -space (i.e. quasi-steady assumption). As a result, the intrinsic orientational dynamics of the particles in \mathbf{p} -space is not captured by either of the models, and the unsteadiness in these models are driven by the unsteady flow dynamics typically at a much larger time scale. However, unlike the GTD, the local-approximation model does not assume the local homogeneity in the background velocity gradient. As such, we shall see that this model has an important advantage over the GTD model (see point (ii) and discussion in §5.2.1).

(ii) *Drift*: Compared to the drift term $Pe_s \langle \mathbf{p} \rangle_g$ in the GTD model, the local approximation model contains extra drift terms, $-\mathbf{V}_{g,c}$, $-\mathbf{V}_{g,u}$, $-\mathbf{V}_{g,D_T}$ and $-\mathbf{V}_{g,\partial T}$, and they originate from the transformation in §3. As described in table 2, these terms originate from the complicated interactions between particles' orientational dynamics and the particles' motility, the advection by the surrounding shear flow and diffusion of particles and the unsteadiness of the prescribed flow field. Since $Pe_s = \epsilon$ in the local approximation, (4.1) suggests that these terms would relatively be less important than the drift term $Pe_s \langle \mathbf{p} \rangle_g$. In this case, the drift term used in the GTD model remains a good approximation. However, if $\langle \mathbf{p} \rangle_g \lesssim O(Pe_s)$, the drift caused by these extra terms becomes important, and, in §5.2.1, we shall demonstrate that such a case does happen in parallel shear flows, especially through $\mathbf{V}_{g,c}$.

(iii) *Diffusion and dispersion*: Further to the given translation diffusion term with the diffusivity $Pe_s \tilde{D}_T (= D_T)$, the local approximation model in (4.1) exhibits the extra terms with the coefficients $\mathbf{D}_{g,c}$ and \mathbf{D}_{D_T} . As discussed in table 2, the former originates from the particles' motility and the latter from the translational diffusion. In particular, $\mathbf{D}_{g,c}$ obtained from (4.2d)

and (3.10) exhibits an interesting similarity to \mathbf{D}_{GTD} from (2.7d) and (2.7e) in the GTD model. In fact, (4.2d) for the local approximation model differs from (2.7d) for the GTD model only by the extra $\mathbf{b}_{GTD} \cdot \mathbf{G}$. Also, the GTD model contains $\mathbf{b}_{GTD} \mathbf{b}_{GTD} \cdot \mathbf{G}/g$ and the enforcement of symmetry for \mathbf{D}_{GTD} in (2.7e) compared to $\mathbf{D}_{g,c}$ in (3.10) for the local approximation model. However, it is important to mention that these differences are a consequence of extending the original GTD theory (Frankel & Brenner 1989) to shear flow (Frankel & Brenner 1991, 1993), and they do not appear compared to the original GTD model (Frankel & Brenner 1989). Having said this, it should be stressed that, in the case of the local approximation model, there is no reason to enforce $\mathbf{D}_{g,c}$ and \mathbf{D}_{DT} to be symmetric, as they are directly derived by approximating the Smoluchowski equation (2.4). As such, the related processes are not necessarily diffusion. More detailed discussion on the matter will follow in §6.2.

(iv) *Stationary and uniformly sheared suspensions*: Having compared the two models, there are special cases where they show stronger similarities. Firstly, if the suspension is quiescent with negligibly small translational diffusivity D_T , the GTD model and the local approximation model are identical (compare the model in §2.2 and that in §4.1). Indeed, in this case, $\mathbf{V}_{g,\star} = 0$, $\mathbf{D}_{g,D_T} = 0$ and $\mathbf{D}_{g,c} = \mathbf{D}_{GTD}$ in (4.1), confirming the physical relevance of the local approximation model proposed in this work. Secondly, if the suspension is immersed into a uniform parallel shear flow with negligible D_T , the only difference at the steady state is between $\mathbf{D}_{g,c}$ and \mathbf{D}_{GTD} . More specifically, the difference arises from the extra $\mathbf{b}_{GTD} \cdot \mathbf{G}$ in (2.7d) and $\mathbf{b}_{GTD} \mathbf{b}_{GTD} \cdot \mathbf{G}/g$ in (2.7e). Therefore, by the zero components in \mathbf{G} , the cross-stream direction component in the tensors $\mathbf{D}_{g,c}$ and \mathbf{D}_{GTD} would be equal in a uniform parallel shear flow. However, as discussed in §2.2, the $\mathbf{b}_{GTD} \cdot \mathbf{G}$ term in (2.7d) can cause singularity in \mathbf{D}_{GTD} if $\text{Re}(\text{eig}(\mathbf{G})) > 0$. (In a parallel shear flow, the singularity does not arise because $\text{Re}(\text{eig}(\mathbf{G})) = 0$.) If the flow is strain-dominant, like the flow near a stagnation point (Bearon *et al.* 2011), then \mathbf{D}_{GTD} might become singular. By contrast, the local approximation does not have this term for $\mathbf{D}_{g,c}$ in (4.2d). Therefore, as long as the orientational dynamics operator \mathcal{L}_p is mathematically well-posed, the local approximation model does not suffer from this issue, offering a significant practical advantage over the GTD model. In the following section, we shall make a more detailed comparison by considering a couple of parallel flow examples.

5. Flow examples

Now, we will test the accuracy of the local approximation model proposed in §4. To this end, we will numerically solve the particle distribution equation of the local approximation model and the GTD model, and their predictions will then be compared with the full analytical and numerical solution to the Smoluchowski equation (2.4). For simplification, we will consider suspension of bottom-heavy motile (i.e. gyrotactic) micro-organisms in one-dimensional parallel shear flows.

5.1. Numerical method

Our numerical method is loosely based on the Spherenfun package (Townsend *et al.* 2016), which utilises the double Fourier sphere (DFS) method to represent the spherical space \mathbf{p} . The method transforms the longitude and latitude coordinates $(\phi, \theta) \in [-\pi, \pi] \times [0, \pi]$ into two independent Fourier space variables. Here, we follow the definition of Townsend *et al.* (2016, p. C405) and define ϕ and θ such that each component of $\mathbf{p} = [p_x, p_y, p_z]^T$ can be written as

$$p_x = \cos \phi \sin \theta, \quad p_y = \sin \phi \sin \theta, \quad p_z = \cos \theta. \quad (5.1)$$

Periodicity in the spherical space was maintained by enforcing the reflectional symmetry in its transformed coefficients (see Townsend *et al.* 2016, p. C406). The $\nabla_{\mathbf{p}} \cdot [\hat{\mathbf{p}}\Psi]$ operation and the \mathbf{p} -dependent part of the $\nabla_{\mathbf{x}} \cdot [\hat{\mathbf{x}}\Psi]$ operation in (2.4) were completely implemented in the spectral space, such that no Fourier transform is necessary during time-marching. Meanwhile, based

on the parallel assumption in the physical space \mathbf{x} , we have only discretised the cross-stream direction (x or z , depending on the prescribed flow field) by a 6th order central difference scheme with an equispaced grid. Time integration was conducted semi-implicitly, in which the $\nabla_{\mathbf{p}}^2$ term was advanced with a second-order Crank-Nicolson method while the rest are marched with a third-order Runge-Kutta method. The matrix inversion arising in the Crank-Nicolson method was solved using the Helmholtz algorithm in the Spherenfun package. For simplicity, we have implemented periodic boundary condition. The method was validated by comparing the \mathbf{p} -space results with a previous solver (Hwang & Pedley 2014b) and with the analytical solution of the following example.

Since the numerical solution of the Smoluchowski equation will be compared with the steady results from the GTD model, we have also computed the drifts and effective diffusivity/dispersion of the two models ((2.7) and (4.2)) by directly inverting the linear $\mathcal{L}_{\mathbf{p}}$ operator in spectral space. The resulting drifts and effective diffusivity/dispersion are then used to solve the steady solutions (see (5.2-5.4)) by direct inversion in the discretised \mathbf{x} -space. The method was also validated with the previous solver used to compute the GTD model (Fung *et al.* 2020).

5.2. A suspension of gyrotactic active particles in a prescribed vertical flow

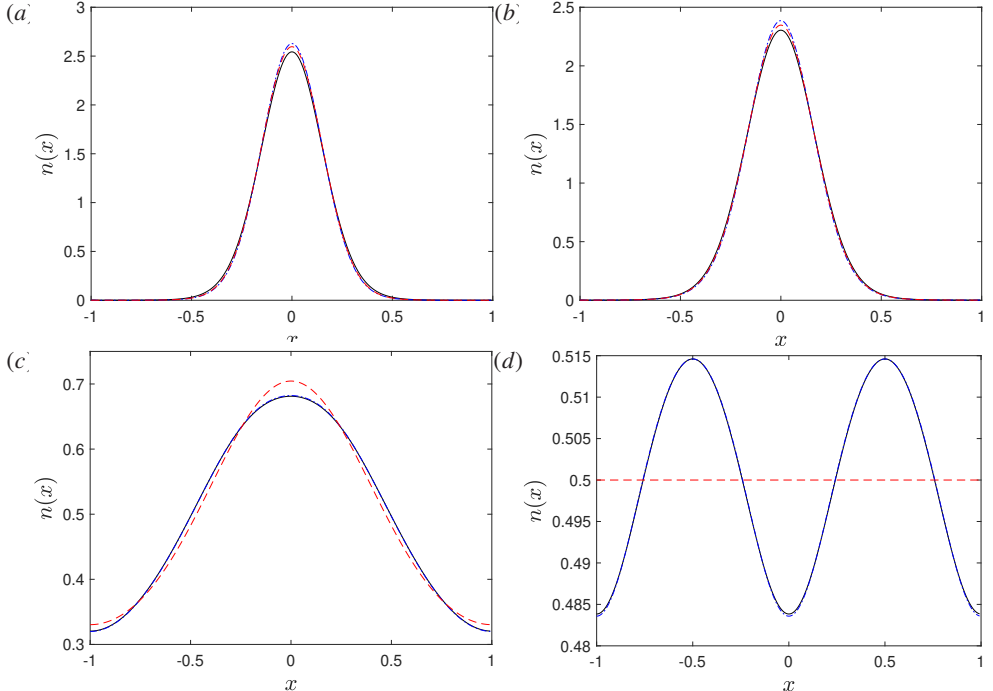


Figure 1: Comparison of the steady-state particle distributions given by the direct integration of (2.4) (black solid line, $n_{f,s}$), the local approximation model of §4 (blue dot-dashed line, $n_{g,s}$) and the GTD model (red dashed line, n_{GTD}) of suspensions of (a) spherical and strongly gyrotactic ($\beta = 2.2$, $\alpha_0 = 0$), (b) non-spherical and strongly gyrotactic ($\beta = 2.2$, $\alpha_0 = 0.31$), (c) non-spherical and weakly gyrotactic ($\beta = 0.21$, $\alpha_0 = 0.31$) and (d) non-spherical and non-gyrotactic ($\beta = 0$, $\alpha_0 = 0.31$) particles. The suspensions are subjected to a vertical flow $W(x) = -\cos(\pi x) - 1$ with $Pe_s = 0.25$ and $Pe_f = 1$.

In this example, we will revisit the classical problem of the formation of the gyrotactic plume (Kessler 1986; Hwang & Pedley 2014a; Jiang & Chen 2020; Fung *et al.* 2020) by bottom-heavy

motile micro-organisms (referred to as particles hereafter). For simplicity, we do not take into account how the particles may influence the flow via buoyancy or hydrodynamic interactions. Instead, we apply a prescribed parallel shear flow to the suspension $\mathbf{u}(\mathbf{x}) = [0, 0, W(x)]^T$, in which x is the horizontal direction and z is the vertical direction pointing upwards (i.e. the same direction as \mathbf{k}).

Four types of idealised motile micro-organisms are considered: a strongly gyrotactic and spherical particle ($\beta = 2.2$, $\alpha_0 = 0$), a strongly gyrotactic but non-spherical particle ($\beta = 2.2$, $\alpha_0 = 0.31$), a weakly gyrotactic non-spherical particle ($\beta = 0.21$, $\alpha_0 = 0.31$) and non-gyrotactic and non-spherical particle ($\beta = 0$, $\alpha_0 = 0.31$). The parameters $\beta = 2.2$ and $\alpha_0 = 0.31$ for the strongly gyrotactic particle is based on *Chlamydomonas augustae* (Pedley & Kessler 1990; Croze *et al.* 2010), while the gyrotactic parameter $\beta = 0.21$ for the weakly gyrotactic particle is based on *Dunaliella salina* (Croze *et al.* 2017). Since we cannot to find any experimental value of α_0 for *D. salina*, we will assume the weakly gyrotactic particle share the same value of $\alpha_0 = 0.31$ for comparisons. Lastly, we have also considered a suspension of non-spherical and non-gyrotactic particles for completeness.

In §5.2.1-5.2.2, we first assume that the gyrotactic particle undergoes no translational diffusion and that the dilute suspension is well described by (2.4) with $D_T = 0$. Later in §5.2.3, we will add translational diffusion (i.e. finite D_T) to the particles to show the extra drift and dispersion that may arise from it. Also, to avoid the additional complication that may arise due to the boundary conditions in the physical space (e.g. wall accumulation of Ezhilan & Saintillan 2015), we will assume a periodicity of $2h^*$ in the x -direction. Therefore, the shear flow profile $W(x)$ is periodic in $x \in [-1, 1]$. For convenience, we shall also define the shear profile $S(x) = -(Pe_f/2)\partial_x W(x)$ with $W(x) = -\cos(\pi x) - 1$. The initial condition of the suspension is given to be uniform in both (\mathbf{x}, \mathbf{p}) -space.

5.2.1. Steady solution and shear trapping

In this subsection, we shall first compare the converged steady state with the prediction from §4 and the GTD model. Figure 1 shows the particle distribution at converged steady state $n_{f,s}$ after the numerical integration of the Smoluchowski equation for the suspensions of the idealised particles. Here, a non-negligibly large value of Pe_s ($\equiv 0.25$) is deliberately chosen to highlight the deviation of the prediction by the local approximation model from the solution to the full Smoluchoski equation. In the case of spherical gyrotactic particle suspension (figure 1a), an analytical solution (B 1) has been found for the steady state of spherical gyrotactic particle suspension in a vertical flow (appendix B) and agrees very well with the numerical solution. In figure 1, we have also plotted the steady-state particle distribution given by the local approximation model in §4 ($n_{g,s}$) and by the GTD theory (n_{GTD}). For strongly gyrotactic particles (figures 1a,b), the two models give predictions very close to the exact results from the direct integration of the Smoluchowski equation, although the GTD model is found to predict slightly better than the local approximation model. However, for weakly gyrotactic particles (figure 1c), the small Pe_s local approximation outperforms the GTD model. Lastly, if the particles are non-spherical and non-gyrotactic, the local approximation makes predictions almost identical to the exact result from the Smoluchowski equation. However, the GTD model fails to predict the aggregation of particles at regions of rapid change of shear rate, giving a uniform distribution instead.

Now, we investigate the performance of the local approximation model and the GTD model in terms of the coefficients of the transport equation given by each model. For a suspension of gyrotactic particles with $D_T = 0$ in a prescribed parallel shear flow, the exact steady solution for the particle distribution $n_{f,s} = n(x, \infty)$ is given from (3.11) by

$$\partial_x [(Pe_s \langle p_x \rangle_g - Pe_s V_{x,c}) n_{f,s}] = Pe_s \partial_x [D_{xx,c} \partial_x n_{f,s}]. \quad (5.2)$$

Similarly, the steady solution to the local approximation model in (4.1), denoted by $n_{g,s}(x)$, is

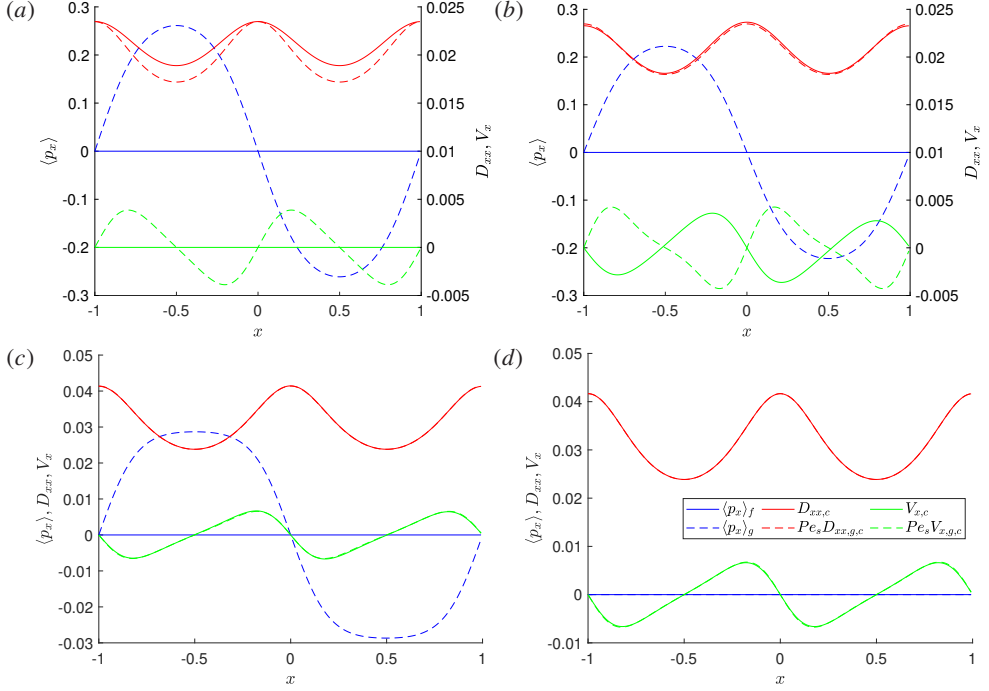


Figure 2: The values of $\langle p_x \rangle_f$ (blue, solid), $\langle p_x \rangle_g$ (blue, dashed), $D_{xx,c}$ (red, solid), $Pe_s D_{xx,g,c}$ (red, dashed), $V_{x,c}$, (green, solid) and $Pe_s V_{x,g,c}$ (green, dashed) at the steady state of a suspension of (a) spherical and strongly gyrotactic ($\beta = 2.2$, $\alpha_0 = 0$), (b) non-spherical and strongly gyrotactic ($\beta = 2.2$, $\alpha_0 = 0.31$), (c) non-spherical and weakly gyrotactic ($\beta = 0.21$, $\alpha_0 = 0.31$) and (d) non-spherical and non-gyrotactic ($\beta = 0$, $\alpha_0 = 0.31$) particles. The suspensions are subjected to a vertical flow $W(x) = -\cos(\pi x)$ with $Pe_s = 0.25$ and $Pe_f = 1$.

given by

$$\partial_x [(Pe_s \langle p_x \rangle_g - Pe_s^2 V_{x,g,c}) n_{g,s}] = Pe_s^2 \partial_x [D_{xx,g,c} \partial_x n_{g,s}]. \quad (5.3)$$

Finally, the steady solution to the GTD model (2.7), $n_{GTD}(x)$, is given by

$$\partial_x [Pe_s \langle p_x \rangle_g n_{GTD}] = Pe_s^2 \partial_x [D_{xx,GTD} \partial_x n_{GTD}]. \quad (5.4)$$

Figure 2 shows the x components of the drift terms and the phenomenological diffusion/dispersion coefficients. First, we compare the phenomenological diffusion/dispersion from the local approximation method and the GTD model with those from the exact transformation (see the right-hand side of (5.2-5.4)). We note from the discussion in §4.2 that $D_{xx,g,c} = D_{xx,GTD}$ for \mathbf{G} considered in this case, as most of its components are zeros: compare $D_{xx,g,c}$ from (4.2d) and (3.10) with $D_{xx,GTD}$ from (2.7d) and (2.7e). Furthermore, when particles are spherical, $D_{xx,c}$ can be directly extracted as a function of the local vertical shear rate S using the analytic solution to (2.4) given in appendix B. In figure 3, $D_{xx,c}$, $D_{xx,g,c}$ and $D_{xx,GTD}$ are plotted as a function of the vertical shear rate S . It is found that $Pe_s D_{xx,g,c}$ (and $Pe_s D_{xx,GTD}$) approximates $D_{xx,c}$ quite well for all the range of S considered. In general, $D_{xx,c}$ remains a good approximation for $D_{xx,g,c}$ for all the four cases considered at all the horizontal location x (figure 2). The good approximation of $D_{xx,c}$ by $Pe_s D_{xx,GTD}$ also explains why the GTD model has consistently been found to outperform the FP model of Pedley & Kessler (1990) (Croze *et al.* 2013, 2017; Fung *et al.* 2020).

As for the left-hand side of (5.2-5.4), all methods share the same $\langle p_x \rangle_g$ term. However, the

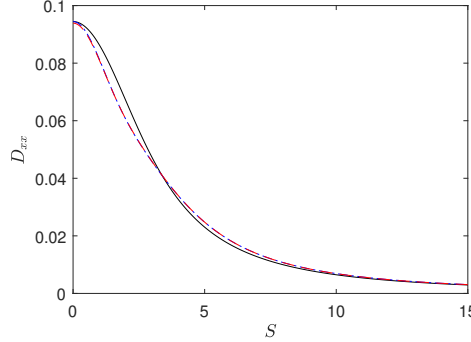


Figure 3: The xx component of \mathbf{D}_c/Pe_s (black line), $\mathbf{D}_{g,c}$ (blue dot-dash line) and \mathbf{D}_{GTD} (red dashed line) as a function of the local vertical shear $S(x)$ for spherical gyrotactic particles ($\beta = 2.2, \alpha_0 = 0$), in which \mathbf{D}_c/Pe_s is computed from $f_s(\mathbf{p})$ of Appendix B. Note that $\mathbf{D}_{g,c}$ overlaps with \mathbf{D}_{GTD} in the figure because they share the same formulae.

local approximation method gives $V_{x,g,c}$ as an approximation of $V_{x,c}$, while GTD does not have an equivalent term. Given that the local approximation model shares the same right-hand side as the GTD model for the x component, the inclusion of $V_{x,g,c}$ becomes the differentiating factor for the performance of the two models in these examples. As shown in figure 2, $V_{x,g,c}$ follows $V_{x,c}$ closely in the weakly gyrotactic cases (figures 2c,d), but poorly in the strongly gyrotactic cases (figures 2a,b). Hence, the local approximation model performs better than the GTD model in figure 1(c), but slightly worse in figures 1(a) and 1(b). However, in the strongly gyrotactic cases, the left-hand side of (5.2) and (5.3) are dominated by $\langle p_x \rangle_g$, so the poor estimation of $V_{x,c}$ does not strongly affect the overall performance of the local approximation model (figures 1c,d).

Given the observation in the weakly gyrotactic cases (figures 2c,d), it would be essential to model the drift term with $\mathbf{V}_{g,c}$ in (4.1) appropriately. Here, we further discuss the importance of this term from a physical perspective. The term $\mathbf{V}_{g,c}$ arises from the inhomogeneity of the local flow field (i.e. shear $S(x)$ in this example). Given the GTD theory assumes a locally homogeneous shear flow (i.e. a quasi-homogeneous assumption), it cannot capture the effect of inhomogeneity in the shear $S(x)$ (see §4.2, point (i)), as is evident from the lack of an equivalent term for $\mathbf{V}_{g,c}$ in (2.7a). The form of (4.2e) for $\mathbf{V}_{g,c}$ suggests that there are two physical mechanisms at play that contribute to $\mathbf{V}_{g,c}$. One is the net flux caused by different levels of gyrotactic drift at different levels of shear at the adjacent location. The flux mainly manifests in the $-g\mathbf{\nabla}_x \cdot \langle \mathbf{p} \rangle_g$ term in (4.2e), which diminishes in the absence of gyrotaxis. The other is the shear trapping mechanism of Bearon & Hazel (2015) and Vennamneni *et al.* (2020), which arises from the ‘eccentric shape’ of the particles. In the presence of inhomogeneous shear, the non-spherical shape leads to some inhomogeneity of g in the \mathbf{x} -space (for the detailed mechanism, see Vennamneni *et al.* 2020). Therefore, having a non-uniform shear in \mathbf{x} -space can lead to non-zero $\mathbf{\nabla}_x g$, even if the particle does not exhibit a biased-motility (i.e. $\langle \mathbf{p} \rangle_g = 0$). This behaviour would primarily manifest in the $\mathbf{p} \cdot \mathbf{\nabla}_x g$ term in (4.2e).

The importance of the drift term with $\mathbf{V}_{g,c}$ can further be understood by examining the scaling of the four cases in figures 1 and 2. In the first case where the particles are spherical and strongly gyrotactic ($\alpha_0 = 0, \beta \sim O(1)$), the form of (4.1) implies $Pe_s^2 V_{x,g,c} \sim O(Pe_s^2)$, an order-of-magnitude smaller than $Pe_s \langle p_x \rangle_g$: i.e. $\langle \mathbf{p} \rangle_g \gg Pe_s V_{x,g,c}$. This behaviour remains the same in the second case where the particles are non-spherical and strongly gyrotactic ($\alpha_0 \neq 0, \beta \sim O(1)$). However, in the third case where the particles are spheroidal and weakly gyrotactic ($\alpha_0 \sim \beta \sim O(Pe_s)$), $\langle p_x \rangle_g \sim Pe_s V_{x,g,c}$ due to $\langle p_x \rangle_g \sim O(Pe_s)$ from $\beta \sim O(Pe_s)$. Hence, if the particles are weakly gyrotactic, $V_{x,g,c}$ is of significance, and the local approximation model

performs better than the GTD model. Lastly, for the spheroidal and non-gyrotactic particles ($\alpha_0 \neq 0, \beta = 0$), $V_{x,g,c}$ becomes dominant while $\langle p_x \rangle_g = 0$. In this case, $V_{x,g,c}$ is purely from the shear trapping mechanism proposed by Bearon & Hazel (2015) and Vennamneni *et al.* (2020). The GTD model then performs very poorly due to the lack of an equivalent term of $V_{x,g,c}$ in (5.4): indeed, n_{GTD} from the GTD model in figure 1(d) gives a uniform distribution even though the exact solution $n_{f,s}$ shows a non-trivial wavy distribution. By the inclusion of the drift term $V_{x,g,c}$, $n_{g,s}$ from the local approximation model recovers the effect of inhomogeneity and gives an excellent prediction for $n_{f,s}$ obtained from the full Smoluchowski equation (figure 1d).

5.2.2. Transient dynamics

In this subsection, we investigate the transient dynamics from the perspective of the exact transformed equation. Rewriting (3.1) for this example, we have

$$\partial_t n + Pe_s \partial_x [\langle p_x \rangle_f n] = 0, \quad (5.5)$$

in which $\langle p_x \rangle_f$ can be expanded through (3.8) into

$$\langle p_x \rangle_f = \langle p_x \rangle_g - V_{x,c} - V_{x,\partial t} - D_{xx,c} \frac{\partial_x n}{n}. \quad (5.6)$$

Substituting (5.6) into (5.5) yields the transport equation

$$\partial_t n + Pe_s \partial_x [(\langle p_x \rangle_g - V_{x,c} - V_{x,\partial t}) n] = \partial_x D_{xx,c} \partial_x n. \quad (5.7)$$

Movies 1-4 show how the balance in (5.6) evolves in time from a uniform suspension. In the beginning, all terms were zeros, except for $\langle p_x \rangle_g$ and the unsteadiness in f which balance out each other. Note that the unsteadiness in f was transformed into a drift $V_{x,\partial t}$ in transport equation (see (4.2f)). As the suspension starts to evolve, the \mathbf{p} -space evolves first in the time scale of order of unity (i.e. the fast time scale in §4) – note that the time scale in the \mathbf{p} -space is $1/d_r^*$ (see §2). The fast-changing f drives the drift $V_{x,\partial t}$ away from $\langle p_x \rangle_g$ in the beginning, resulting in non-zero $\langle p_x \rangle_f$ in (5.6), which in turn generates the unsteadiness in n in (5.5). Therefore, $n(x, t)$ does not start evolving until $V_{x,\partial t}$ has become significantly different from $\langle p_x \rangle_g$. For $t \gtrsim O(1)$, $V_{x,\partial t}$ is close to zero, indicating that f has reached the quasi-steady regime, justifying the assumption of §4. It is also in this time interval where $V_{x,c} \approx V_{x,g,c}$ and $D_{xx,c} \approx D_{xx,g,c}$, implying that the local approximation in §4 would be valid after this short initial transient.

For $t \gtrsim O(1)$, $n(x, t)$ evolves slowly, while $\langle p_x \rangle_f$ diminishes towards zero, mainly due to the increasing magnitude of $(\partial_x n/n)$ to balance $\langle p_x \rangle_g$ in (5.6). As $\langle p_x \rangle_f$ vanishes, $n(x, t)$ reaches steady equilibrium. During this slow transient period, f also evolves slowly, but slow enough such that $V_{x,\partial t}$ remains insignificant. Note that, in this example, the prescribed flow field was steady, such that $V_{x,g,\partial T}$ vanishes. If the prescribed flow were unsteady in the long timescale T , we would also expect $V_{x,\partial t}$ to be significant and to be well approximated by $V_{x,g,\partial T}$. In all the examples considered, $D_{xx,c}$ remains close to the approximation $D_{xx,g,c}$. In weakly and non-gyrotactic suspensions, $V_{x,c}$ does not evolve far from $V_{x,g,c}$ either, but in strongly gyrotactic suspension, $V_{x,c}$ is found to change direction as $t \rightarrow \infty$. As mentioned in §5.2.1, $V_{x,c}$ is considerably small compared to $\langle p_x \rangle_g$ in this case. Therefore, regardless of the fact that $V_{x,g,c}$ differs from $V_{x,c}$, the local approximation model still performs well.

5.2.3. Translational diffusion

Lastly, we will consider non-zero translational diffusion for the previous examples. Micro-algae such as *Chlamydomos* and *Dunaliela* are often considered to have negligible thermal diffusion given their relatively large sizes (see reviews by Pedley & Kessler 1992; Saintillan 2018; Bees 2020). While their random walk is often modelled only through the rotational diffusion by assuming that the intra-cellular biochemical noise only affects the rotational motion,

in theory, there is no reason that the randomness can be modelled solely through the rotational diffusion without translational diffusion because the swimming mechanisms very often involve sophisticated noisy beating dynamics of cilia and flagella (e.g. Wan & Goldstein 2014). Given the ambiguity in choosing a biologically relevant value of D_T , here we will simply consider some values for D_T to demonstrate the role of D_T in the transport equation, i.e. ∇_{D_T} and \mathbf{D}_{D_T} .

We consider the steady-state particle distribution at an arbitrary value of $D_T = 0.01$, which is chosen to be of similar magnitude as $Pe_s \mathbf{D}_c$. This arbitrary choice was made to highlight the potential role of the translational diffusion. Also, for biological micro-particles, any D_T value larger than $Pe_s \mathbf{D}_c$ would be physically unrealistic (c.f. experimental measurements of Croze *et al.* (2017)). We have also computed the steady-state at $D_T = 0.002$, but since the results are qualitatively the same, we shall only present the $D_T = 0.01$ case here.

The exact steady-state particle distribution $n_{f,s}(x)$ from the Smoluchowski equation (2.4) is given by

$$\partial_x[(Pe_s \langle p_x \rangle_g - Pe_s(V_{x,c} + V_{x,D_T}))n_{f,s}] = \partial_x[(D_T + Pe_s(D_{xx,c} + D_{xx,D_T}))\partial_x n_{f,s}], \quad (5.8)$$

and the one for the local approximation model $n_{g,s}$ derived in §4 is given by

$$\partial_x[(Pe_s \langle p_x \rangle_g - Pe_s^2(V_{x,g,c} + V_{x,g,D_T}))n_{g,s}] = \partial_x[(D_T + Pe_s^2(D_{xx,g,c} + D_{xx,g,D_T}))\partial_x n_{g,s}]. \quad (5.9)$$

Note that $Pe_s^2 V_{x,g,D_T}$ and $Pe_s^2 D_{xx,g,D_T}$ scale with $Pe_s D_T$ from (4.2b) and (4.2c). Meanwhile, n_{GTD} is given by

$$\partial_x[Pe_s \langle \mathbf{p} \rangle_g n_{GTD}] = \partial_x[(D_T + Pe_s^2 D_{xx,GTD})\partial_x n_{GTD}]. \quad (5.10)$$

As shown before in §4.2, the GTD model gives $D_{xx,GTD} = D_{xx,g,c}$. However, it does not offer any approximations for $V_{x,c}$, V_{x,D_T} and D_{xx,D_T} . Therefore, any difference between $n_{g,s}$ and n_{GTD} has to come from $V_{x,g,c}$, V_{x,g,D_T} and D_{x,g,D_T} .

Figure 4 shows the steady-state particle distributions with $D_T = 0.01$ for the same parameters considered in figure 1. One can see that the introduction of non-zero D_T has further smoothed out the particle distributions in all cases considered by comparing figures 1 and 4. However, D_T does not seem to have significantly altered most of the conclusions drawn in §5.2.1, except that the local approximation model now performs better than the GTD model even in strongly gyrotactic suspensions. This improved performance can be attributed to several factors. Firstly, $V_{x,c}$ becomes closer to the approximation $V_{x,g,c}$ in strongly gyrotactic suspensions in the presence of D_T , as shown by figures 5(a,b) in comparison with figures 2(a,b). Secondly, D_T gives rise to V_{x,D_T} (cyan solid lines in figure 5), which can be as large in magnitude as $V_{x,c}$ in strongly gyrotactic cases (figures 5a,b). Since the GTD model does not contain either ∇_c or ∇_{D_T} , the inclusion of $V_{x,g,c}$ and V_{x,g,D_T} approximating $V_{x,c}$ and V_{x,D_T} gives a better performance of the local approximation model. Thirdly, the introduction of D_T also gives rise to D_{xx,D_T} (magenta solid lines in figure 5). Despite being not as large as $D_{xx,c}$ overall, D_{xx,D_T} has variations over x comparable to that of $D_{xx,c}$ (magenta and red solid lines in figure 5). Therefore, the local approximation model, which contains the terms with $V_{x,g,c}$, V_{x,g,D_T} and D_{x,g,D_T} , predicts particle distributions better than the GTD model.

Comparing the strongly gyrotactic (figure 5b) with the weakly gyrotactic case (figure 5c), one can also conclude that the effect of V_{x,D_T} and D_{xx,D_T} are much stronger in strongly gyrotactic suspensions. Since V_{x,D_T} and D_{xx,D_T} are driven by $\nabla_x f$ and $\nabla_x^2 f$ according to (3.4b) and (3.4c), the large V_{x,D_T} and D_{xx,D_T} are likely driven by larger variation of f in x induced by the stronger gyrotaxis.

Lastly, it is worth noting that D_{xx,D_T} and D_{xx,g,D_T} can be negative for some domain in x . As mentioned in §3, the terms with D_{xx,D_T} and D_{xx,g,D_T} do not necessarily represent diffusion – they depict dispersive behaviour introduced by translational diffusion. Therefore, negative diagonal values in \mathbf{D}_{D_T} are allowed, and they physically represent possible particle aggregation

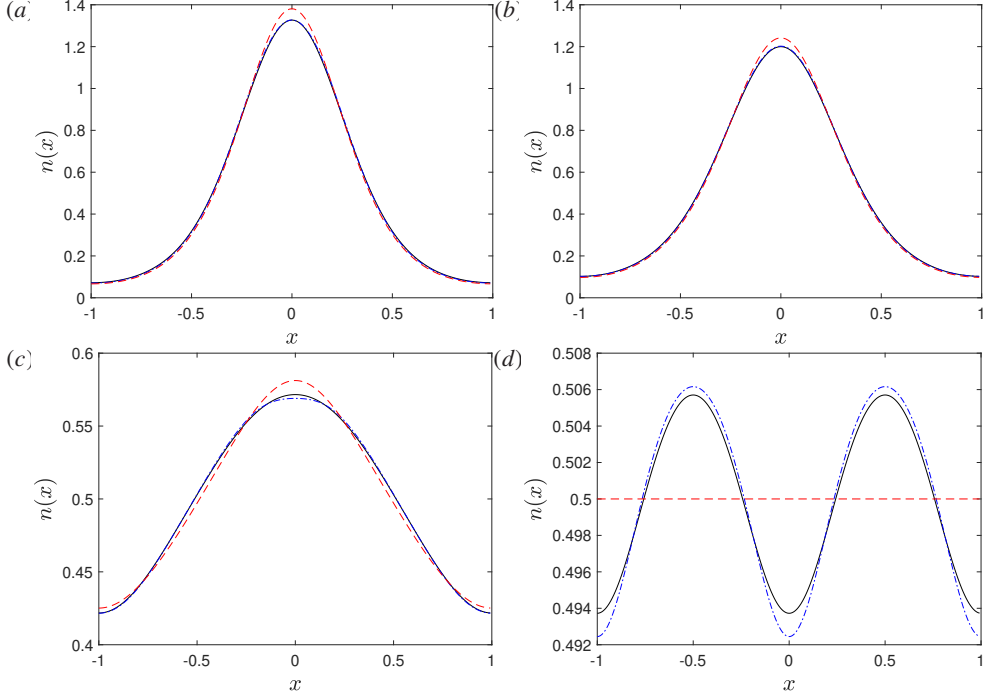


Figure 4: Comparison of the steady-state particle distributions given by the direct integration of (2.4) (black solid line, $n_{f,s}$), the local approximation of §4 (blue dot-dashed line, $n_{g,s}$) and the GTD model (red dashed line, n_{GTD}) of suspensions of (a) spherical and strongly gyrotactic ($\beta = 2.2$, $\alpha_0 = 0$), (b) non-spherical and strongly gyrotactic ($\beta = 2.2$, $\alpha_0 = 0.31$), (c) non-spherical and weakly gyrotactic ($\beta = 0.21$, $\alpha_0 = 0.31$) and (d) non-spherical and non-gyrotactic ($\beta = 0$, $\alpha_0 = 0.31$) particles. The particles are diffusive such that $D_T = 0.01$. The suspensions are subjected to a vertical flow $W(x) = -\cos(\pi x) - 1$ with $Pe_s = 0.25$ and $Pe_f = 1$.

due to interaction between the cross-dispersion between n and f due to \mathbf{x} -space diffusion and the particles' orientational dynamics (see (3.4c) and table 2). The same interpretation can also be applied to the approximation \mathbf{D}_{g,D_T} . More discussion on the implication of the these dispersion tensors will follow in §6.2.

5.3. A suspension of gyrotactic active particles subjected to a prescribed horizontal flow

In this section, we consider a horizontal shear flow $\mathbf{u} = [U(z), 0, 0]^T$ in the gyrotactic suspension instead of a vertical shear flow. Similar to §5.2, we first assume an infinite \mathbf{x} -domain with a periodicity in z and no translational diffusion. The horizontal shear flow is prescribed as $U(z) = \cos(\pi z)$. We also introduce the shear profile $S(z) = (Pe_f/2)\partial_z U(z)$. As noted in §4.2, the cross-stream dispersion $D_{zz,g,c}$ from the local approximation is the same as $D_{zz,GTD}$ from the GTD model. It is similar to how $D_{xx,g,c} = D_{xx,GTD}$ in the vertical shear case. Figure 6(a) shows that the steady-state particle distribution profile $n(z)$ for strongly gyrotactic suspension ($\beta = 2.2, \alpha_0 = 0.31$) computed from the local approximation model and the GTD model is similar. Similar to the case studied in §5.2.1, the small differences come from the presence of $V_{z,g,c}$, which is relatively small when compared to $\langle \mathbf{p} \rangle_g$ (figure 7a). However, in figure 6(b), the steady-state particle distribution profile $n(z)$ for weakly gyrotactic non-spherical particles ($\beta = 0.21, \alpha_0 = 0.31$) computed from the local approximation model is more accurate than that of the GTD model due to the presence of $V_{z,g,c}$, which is consistent with the prediction of §4.2.

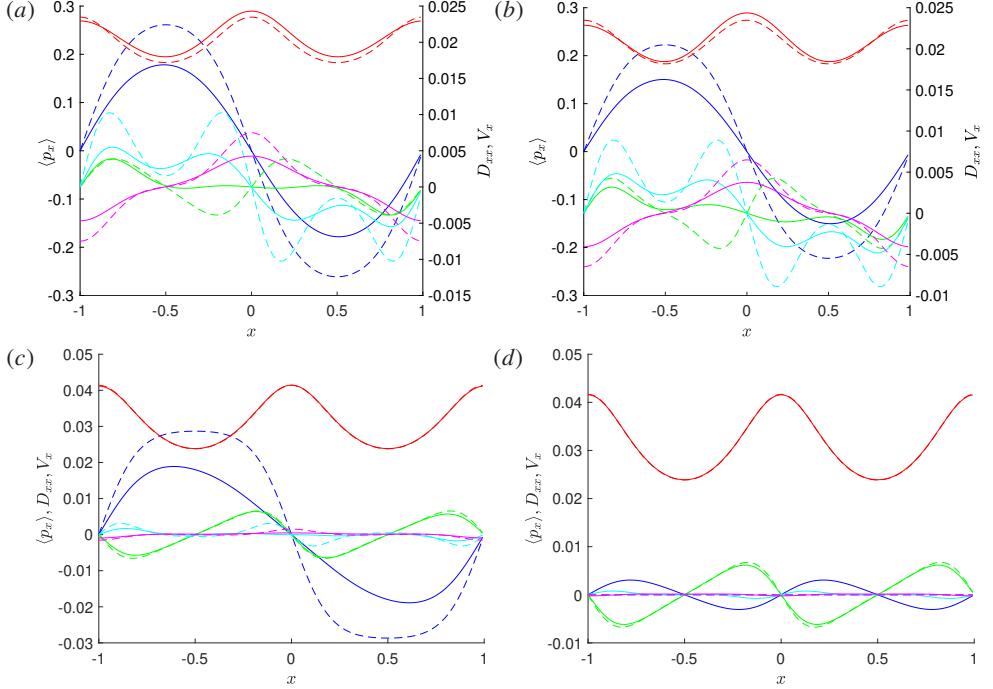


Figure 5: The values of $\langle p_x \rangle_f$ and $\langle p_x \rangle_g$ (blue), $D_{xx,c}$ and $Pe_s D_{xx,g,c}$ (red), $V_{x,c}$ and $Pe_s V_{x,g,c}$ (green), D_{xx,D_T} and $Pe_s D_{xx,g,D_T}$ (magenta), V_{x,D_T} and $Pe_s V_{x,g,D_T}$ (cyan) calculated using the steady-state $f(\mathbf{x}, \mathbf{p}, \infty)$ (solid lines) and $g(\mathbf{x}, \infty; \mathbf{p})$ (dashed lines) of a suspension of (a) spherical and strongly gyrotactic ($\beta = 2.2$, $\alpha_0 = 0$), (b) non-spherical and strongly gyrotactic ($\beta = 2.2$, $\alpha_0 = 0.31$), (c) non-spherical and weakly gyrotactic ($\beta = 0.21$, $\alpha_0 = 0.31$) and (d) non-spherical and non-gyrotactic ($\beta = 0$, $\alpha_0 = 0.31$) particles. The particles are diffusive such that $D_T = 0.01$. The suspensions are subjected to a vertical flow $W(x) = -\cos(\pi x) - 1$ with $Pe_s = 0.25$ and $Pe_f = 1$.

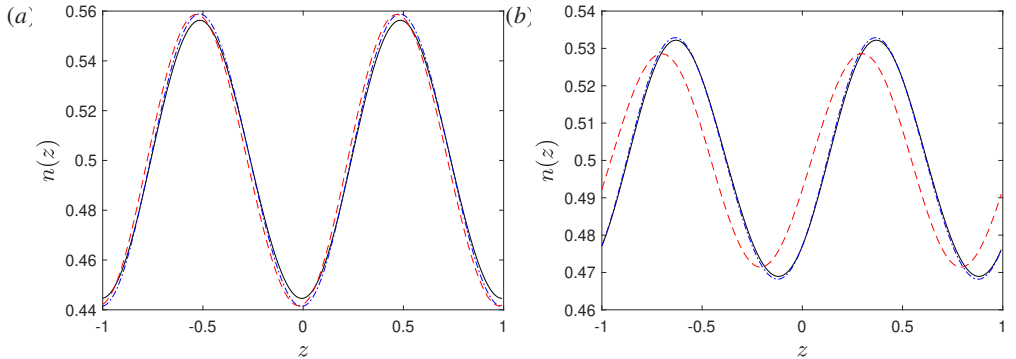


Figure 6: Comparison of the steady-state particle distributions given by the direct integration of (2.4) (black solid line, $n_{f,s}$), the local approximation of §4 (blue dot-dashed line, $n_{g,s}$) and the GTD model (red dashed line, n_{GTD}) of suspensions of (a) strongly gyrotactic particles ($\beta = 2.2$, $\alpha_0 = 0.31$) and (b) weakly gyrotactic particles ($\beta = 0.21$, $\alpha_0 = 0.31$). The suspensions are subjected to horizontal shear flow $U(z) = \cos(\pi z)$ with $Pe_s = 0.25$ and $Pe_f = 1$.

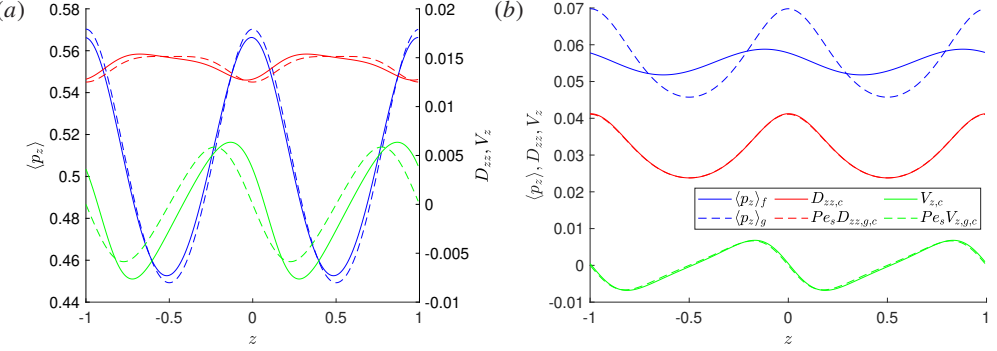


Figure 7: The values of $\langle p_z \rangle_f$ (blue, solid), $\langle p_z \rangle_g$ (blue, dashed), $D_{zz,c}$ (red, solid), $Pe_s D_{zz,g,c}$ (red, dashed), $V_{z,c}$, (green, dashed) and $Pe_s V_{z,g,c}$ (green, solid) at the steady state of a suspension of (a) strongly gyrotactic particles ($\beta = 2.2$, $\alpha_0 = 0.31$) and (b) weakly gyrotactic particles ($\beta = 0.21$, $\alpha_0 = 0.31$). The suspensions are subjected to a horizontal shear flow $U(z) = \cos(\pi z)$ with $Pe_s = 0.25$ and $Pe_f = 1$.

The explanation for the better performance of the local approximation method is the same as that in §5.2.1, in which the inclusion of $V_{z,g,c}$ is significantly improving the prediction from the local approximation (figure 7b).

The transient dynamics is also investigated for the horizontal flow. As shown in movies 5-6, the simulation initially shows the dominant balance between $V_{z,\partial t}$ and $\langle p_z \rangle_g$. At the time scale of order unity, $V_{z,\partial t}$ diminishes quickly, driven by the fast-changing f . At $t \gtrsim O(1)$, $V_{z,\partial t}$ becomes insignificant, indicating that f has reached the quasi-steady regime. Meanwhile, the local approximation accurately predicts $V_{z,c} \approx V_{z,g,c}$ and $D_{zz,c} \approx D_{zz,g,c}$, similar to how $V_{x,c} \approx V_{x,g,c}$ and $D_{xx,c} \approx D_{xx,g,c}$ in §5.2.2. However, unlike the vertical flow cases, movies 5-6 show that $\langle p_z \rangle_f$ does not tend to zero as $t \rightarrow \infty$ in these horizontal flow cases. Instead, figure 7 shows that they stay in roughly the same order as $\langle p_z \rangle_g$ at steady equilibrium. Moreover, both $V_{z,g,c}$ and $D_{zz,g,c}$ remains good approximations to $V_{z,c}$ and $D_{zz,c}$ respectively for a long time, even when particles are strongly gyrotactic. Therefore, when the flow is horizontal, the local approximation model outperforms the GTD even in strongly gyrotactic suspensions.

6. Discussion

6.1. Physical implication of the transformation

This work sets out to seek a model transport equation that can predict the particle distribution given by the Smoluchowski equation without solving the equation directly. To achieve the goal, in §3, we have shown how the Smoluchowski equation (2.4) can be transformed into a transport equation by expanding $\langle \mathbf{p} \rangle_f n$ in the integrated equation (3.1) into $\langle \mathbf{p} \rangle_g n$ and other drifts $\mathbf{V}_\star n$ and dispersions/diffusions $\mathbf{D}_\star \nabla_{\mathbf{x}} n$. This expansion of $\langle \mathbf{p} \rangle_f$ contrasts with the GTD model, which takes the averaged orientation $\langle \mathbf{p} \rangle_g$ of individual particle directly as the drift.

To better show the implication of this transformation, here we rewrite the procedures in §3 under the assumption of parallel flow and $D_T = 0$. We can rewrite (3.1) as

$$\partial_t n(\mathbf{x}, t) + \nabla_{\mathbf{x}} \cdot [(\mathbf{Pe}_s \langle \mathbf{p} \rangle_f(\mathbf{x}, t) n) = 0, \quad (6.1)$$

in which $\langle \mathbf{p} \rangle_f n$ can be expanded through (3.8) or

$$\langle \mathbf{p} \rangle_f = \langle \mathbf{p} \rangle_g - \mathbf{V}_c - \mathbf{V}_{\partial t} - \mathbf{D}_c \frac{\nabla_{\mathbf{x}} n}{n}, \quad (6.2)$$

into the transport equation

$$\partial_t n + Pe_s \nabla_{\mathbf{x}} \left[(\langle \mathbf{p} \rangle_g - \mathbf{V}_c - \mathbf{V}_{\partial t}) n \right] = \nabla_{\mathbf{x}} \cdot \mathbf{D}_c \nabla_{\mathbf{x}} n. \quad (6.3)$$

Note that equations (6.1-6.3) are the equivalent of (5.5-5.7) in a multi-dimensional coordinate. Now, equation (6.1) and the rewritten equation (6.3) yield two different interpretations of ABPs transport. In (6.1), particles are purely advected by the Eulerian motility flux $Pe_s \langle \mathbf{p} \rangle_f n$, which is the ensemble-averaged flux of particles coming in and out of a certain control volume at position \mathbf{x} due to the motility of the particle. The flux depends on the orientational and spatial distribution of particles inside and at the vicinity of the control volume. However, in (6.3), the average Eulerian motility flux $Pe_s \langle \mathbf{p} \rangle_f n$ is decomposed into the flux from the average motility of individual particles $Pe_s \langle \mathbf{p} \rangle_g n$, the advective flux due to unsteadiness in particles' orientational dynamics $-Pe_s \mathbf{V}_{\partial t} n$, the shear trapping flux $-Pe_s \mathbf{V}_c n$ and the dispersion flux $Pe_s \mathbf{D}_c \nabla_{\mathbf{x}} n$.

It is evident from (6.2) that the average Eulerian motility flux $Pe_s \langle \mathbf{p} \rangle_f n$ is different from the flux of the average motility of individual particles $Pe_s \langle \mathbf{p} \rangle_g n$. However, it might also be counterintuitive at first glance to decipher their differences. Here, the average motility of individual particles $Pe_s \langle \mathbf{p} \rangle_g$ is defined as the ensemble average of the self-propelling velocity of individual particles when subjected to the local velocity gradient or other local factors that may influence their orientation (e.g. taxes). The average motility of individual particles $Pe_s \langle \mathbf{p} \rangle_g$ is based on the average orientation of individual particles $\langle \mathbf{p} \rangle_g$, which is calculated from the homogeneous solution (g) to the operator \mathcal{L}_p , representing the orientational dynamics of individual particles. It is a function of the local velocity gradient and the particles' property only and is independent of any (\mathbf{x}, t) -space configuration. In other words, $\langle \mathbf{p} \rangle_g$ is calculated when the orientational dynamics (\mathcal{L}_p) is decoupled from the rest of the Smoluchowski equation. The resulting average motility $Pe_s \langle \mathbf{p} \rangle_g$ provides a Langrangian view of each individual's motility after being averaged in the local \mathbf{p} -space. Therefore, the average motility flux $Pe_s \langle \mathbf{p} \rangle_g n$ at each (\mathbf{x}, t) depends only on the local velocity gradient at the specified location.

By contrast, the average Eulerian flux $Pe_s \langle \mathbf{p} \rangle_f n$ does consider the spatial and orientational distribution of particles at the nearby location in the (\mathbf{x}, t) -space. It is the result of averaging the particles' motility $Pe_s \mathbf{p} \Psi$ in the Smoluchowski equation (2.4). It includes the flux from the average motility of individuals $Pe_s \langle \mathbf{p} \rangle_g n$ and other fluxes from drifts and dispersions arising from the interaction between the orientational dynamics (\mathcal{L}_p) and the rest of the Smoluchowski equation. For example, it includes the effect of the different orientation distribution at the nearby location, which gives rise to the extra shear trapping flux $-Pe_s \mathbf{V}_c n$, even when the average motility $Pe_s \langle \mathbf{p} \rangle_g$ is zero (as demonstrated in §5.2.1, figure 2d). It also includes the effect of the changing orientation over time, which interacts with the orientational dynamics and manifests as the extra flux $-Pe_s \mathbf{V}_{\partial t} n$ through the particles' motility. Lastly, it includes the dispersion flux $Pe_s \mathbf{D}_c \nabla_{\mathbf{x}} n$, which arises from the distribution of how the particles' instantaneous motilities are different from the averaged motility of the particles in the control volume. All the above extra drifts and dispersions are dependent on the configuration of the suspension in (\mathbf{x}, t) -space (c.f. §5.2.2), in contrast to $Pe_s \langle \mathbf{p} \rangle_g$. Therefore, one may interpret $Pe_s \langle \mathbf{p} \rangle_g$ as the Langrangian view of each individual's motility and $Pe_s \langle \mathbf{p} \rangle_f$ as the Eulerian view of the overall drift of all the particles in the suspension at the given location due to the particles' motility.

The fact that $\langle \mathbf{p} \rangle_g$ is part of $\langle \mathbf{p} \rangle_f$ in (6.2) physically implies that the averaged motility of individuals only contributes to part of the overall Eulerian drift caused by particles' motility. It also indicates that particles dispersion physically comes from the same Eulerian motility flux $Pe_s \langle \mathbf{p} \rangle_f n$ that includes the effect of other drifting terms. This physical perspective is in stark contrast to that of the GTD model. The GTD model takes $Pe_s \langle \mathbf{p} \rangle_g n$ directly as the overall motility flux from its approximation of the temporal growth rate of the first statistical moment (mean), which is effectively using $Pe_s \langle \mathbf{p} \rangle_g n$ as a first-order approximation to $Pe_s \langle \mathbf{p} \rangle_f n$. Because of this, it does not capture the drifts like \mathbf{V}_c and $\mathbf{V}_{\partial t}$. Meanwhile, the effective diffusivity $Pe_s^2 \mathbf{D}_{GTD}$

is found by asymptotically matching it with the temporal growth rate of the second statistical moment (variance). Therefore, in the GTD derivation, it is hard to follow how $Pe_s^2 \mathbf{D}_{GTD}$ arises from the particles' motility. On the contrary, the transformation introduced in this study has directly shown how the dispersion arises from the motility of the particle.

Extending the decomposition to a more general ABP suspension, the passive advection and translation diffusion of particles shall also interact with the orientational dynamics and give rise to extra drifts and dispersion through the particles' motility. Indeed, the interactions give rise to \mathbf{V}_u , \mathbf{V}_{D_T} and \mathbf{D}_{D_T} , which has already been introduced in §3. Their physical meanings are summarised in table 2.

6.2. Non-trivial phenomenological dispersion

In §3 and §4.2, we have briefly highlighted that \mathbf{D}_c and \mathbf{D}_{D_T} , and their respective approximation $\mathbf{D}_{g,c}$ and \mathbf{D}_{g,D_T} , are not necessarily positive definite and symmetric, as they are directly obtained through the Smoluchowski equation (2.4). In fact, there is no reason that the dispersive behaviour of suspensions originating from the orientational dynamics of each ABP would need to solely be described by a 'diffusion' process. This is in contrast to the effective diffusivity \mathbf{D}_{GTD} of the GTD model, which was artificially forced to be positive definite and symmetric (Frankel & Brenner 1991, 1993).

In §5.2.3, we have also shown that the translational diffusion D_T in the Smoluchowski equation (2.4) can give rise to negative xx components in \mathbf{D}_{D_T} and \mathbf{D}_{g,D_T} . In this subsection, we shall further demonstrate that $\mathbf{D}_{g,c}$ is indeed asymmetric, in contrast to the positive definite \mathbf{D}_{GTD} . Focussing on spherical particles, here we shall show that $\mathbf{D}_{g,c}$ caused by dispersion is not necessarily symmetric.

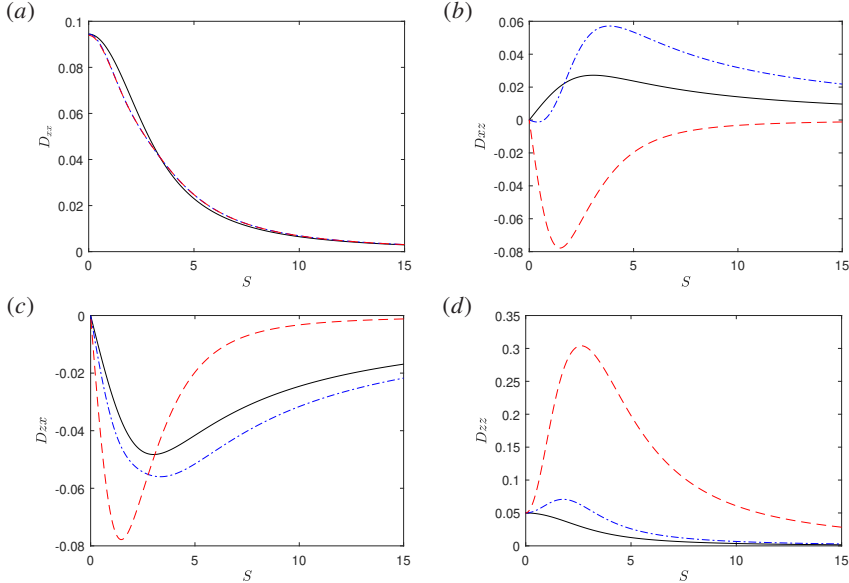


Figure 8: Comparisons of the components of \mathbf{D}_c/Pe_s (black line), $\mathbf{D}_{g,c}$ (blue dot-dash line) and \mathbf{D}_{GTD} (red dashed line) as a function of the local vertical shear $S(x)$ for a suspension of spherical gyrotactic particles ($\beta = 2.2, \alpha_0 = 0$), in which \mathbf{D}_c/Pe_s is computed from $f_s(\mathbf{p})$ of appendix B.

Figure 8 shows a component-wise comparison between \mathbf{D}_c , $\mathbf{D}_{g,c}$ and \mathbf{D}_{GTD} as a function of the local shear rate $S(x)$ for a suspension of idealised spherical ($\alpha_0 = 0$) gyrotactic particles (with

$\beta = 2.2$) in a vertical shear flow. Here, in general, \mathbf{D}_c obtained through the transformation is not a function of the local shear S alone as \mathbf{D}_c is computed from $f(\mathbf{x}, \mathbf{p}, t)$. However, as shown in appendix B, for the particular case of a spherical gyrotactic particle suspension in vertical shear and at steady equilibrium, \mathbf{D}_c/Pe_s can be written as a function of $S(x)$. The calculation of $\mathbf{D}_{g,c}$ and \mathbf{D}_{GTD} are performed per value of S using the numerical scheme detailed in Fung *et al.* (2020).

The comparison shows that \mathbf{D}_c and the approximation $\mathbf{D}_{g,c}$ are highly asymmetric compared to the symmetric diffusivity tensor from GTD, when the shear rate is not zero. These non-symmetric dispersion tensors indicate that the diffusion process would not be the best physical description of ABPs' random walk. Instead, this work considers them as dispersions in the (\mathbf{x}, \mathbf{p}) -space, analogous to the original Taylor-Aris dispersion (Taylor 1953; Aris & Taylor 1956). In the Taylor-Aris dispersion, the cross-stream diffusion gives rise to additional streamwise dispersion through the shear flow. Similarly, in ABP suspensions, the rotational diffusion (in \mathbf{p} -space) gives rise to translational dispersion (in \mathbf{x} -space) through the particles' motility. While the extra streamwise dispersion in Taylor-Aris dispersion is sometimes referred to as 'effective diffusivity' (see Cussler 2009, §4.5), it is not a physical diffusion caused by a translational random walk, but the result of the combination of cross-stream diffusion and a shear flow. Similarly, the 'effective diffusivity' \mathbf{D}_c here is not a diffusion from translational random walk, but the result of the interplay between particles' orientational dynamics and motility. Therefore, \mathbf{D}_c and the approximation $\mathbf{D}_{g,c}$ do not necessarily have to conform to the symmetric and positive definite requirement of a physical diffusivity. A similar argument can be applied to \mathbf{D}_{D_T} and \mathbf{D}_{g,D_T} , which explains why they can have negative xx component in §5.2.3. This interpretation of \mathbf{D}_c and $\mathbf{D}_{g,c}$ contrasts the approach by the generalised Taylor dispersion model, in which the effective diffusivity \mathbf{D}_{GTD} was obtained by the temporal asymptotic growth rate of the statistical variance of particle distribution using the classical definition of diffusion. In this case, by definition, \mathbf{D}_{GTD} must be positive definite and symmetric.

Given the non-trivial nature of the dispersion shown in figure 8, it would be interesting to extend the present work to more complex multi-dimensional flows instead of the current one-dimensional parallel flow. This issue is beyond the scope of the present study, and there is an on-going work to address this issue in the near future.

7. Concluding remarks

In this study, we have proposed a new method to reduce the Smoluchowski equation into a simpler transport equation. The Smoluchowski equation governs the statistics of the position and orientation of ABPs, whose orientational trajectories are described by the Jeffrey orbit in the presence of rotational random noise. The framework is directly applicable to dilute suspensions of ABPs in a large-scale system with strong flow, such as microalgae in the ocean. It can also be extended to the flow regime where the long-range hydrodynamic contribution of swimming motion of individual particles can be represented by averaged stress tensors (e.g. Batchelor 1970; Hinch & Leal 1972a,b; Pedley & Kessler 1990).

We have presented a method to transform the Smoluchowski equation into a transport equation exactly for a given flow field. The method involves decomposing the average Eulerian motility flux $Pe_s \langle \mathbf{p} \rangle_f n$ at a fixed location into the flux from the average Langrangian motility flux of individual particles $Pe_s \langle \mathbf{p} \rangle_g n$ and other contributions. The transformation has shown that $Pe_s \langle \mathbf{p} \rangle_g$ is different from $Pe_s \langle \mathbf{p} \rangle_f$ and only constitutes part of $Pe_s \langle \mathbf{p} \rangle_f$. The transformation also unveils the explicit form of the other drift and dispersion terms contributing to the overall average Eulerian motility. These terms include the shear trapping drift \mathbf{V}_c and the particle dispersion \mathbf{D}_c due to rotational diffusion. In addition, we have also discovered the drift $\mathbf{V}_{\partial t}$ due to the interaction between the unsteadiness in orientation and the orientational dynamics itself, the drift \mathbf{V}_{D_T} and dispersion

\mathbf{D}_{D_T} arise from the interaction between translational diffusion and the orientational dynamics, and the drift \mathbf{V}_u from the interaction between passive advection of orientational distribution and the orientational dynamics.

Although the transformation has revealed these new physical drifts and dispersions are easily interpretable in a transport equation, they cannot be directly used as a model due to the prerequisite to first obtain $\Psi(\mathbf{x}, \mathbf{p}, t)$ by solving the Smoluchowski equation directly. In this regard, this work has presented a new model based on the local approximation of the transformation, which only relies on the local flow information instead of the global flow configuration. By assuming that the time scale of the orientational dynamics is much faster than that of the spatial dynamics, we have approximated the orientational space probability density function $f(\mathbf{x}, \mathbf{p}, t) = \Psi/n$ by the homogeneous solution $g(\mathbf{x}, t; \mathbf{p})$ of the orientational space operator \mathcal{L}_p , thereby circumventing the need to solve for Ψ . The approximation gives the same shear trapping drift $\mathbf{V}_{g,c}$ and the particle dispersion $\mathbf{D}_{g,c}$ as that of Bearon & Hazel (2015) and Vennamneni *et al.* (2020) when the particles have no taxes and diffusion, but it is also extendible to particles with taxes or translational diffusion. We have also made connections between $\mathbf{D}_{g,c}$ and the effective diffusivity \mathbf{D}_{GTD} from the GTD model. In a quiescent flow, the two tensors are equal. When the prescribed flow is parallel, $\mathbf{D}_{g,c}$ and \mathbf{D}_{GTD} share the same cross-stream component (the xx component in verticle shear flows $\mathbf{u} = [0, 0, W(x)]^T$ and zz component in horizontal shear flows $\mathbf{u} = [U(z), 0, 0]^T$). The comparison between the two models also highlighted the missing shear trapping drift $\mathbf{V}_{g,c}$ and the drift \mathbf{V}_{D_T} and dispersion \mathbf{D}_{D_T} from translational diffusion in the GTD model. In particular, when the first-order drift $Pe_s \langle \mathbf{p} \rangle_g$ is small, the second-order drift from $Pe_s^2 \mathbf{V}_{g,c}$ can become significant.

The numerical examples of suspensions in horizontal and vertical shear flows have further illustrated the importance to include $\mathbf{V}_{g,c}$. When $\langle \mathbf{p} \rangle_g$ from gyrotaxis is small, the local approximation method better predicts the particle distribution than the GTD model. In the extreme case where $\langle \mathbf{p} \rangle_g = 0$, the GTD model would give an unphysical uniform distribution while the local approximation can accurately capture the shear trapping phenomena. Meanwhile, when $D_T \neq 0$, the local approximation method has also shown better prediction than the GTD model because of the inclusion of \mathbf{V}_{g,D_T} and \mathbf{D}_{g,D_T} in addition to \mathbf{V}_c . Overall, this work has shown that the local approximation method is either on-par with or better than the GTD model for approximation of particles transport.

Moreover, in the numerical examples, we have demonstrated the possibility of having negative values in D_{xx,D_T} (or D_{xx,g,D_T}). Later, we have also demonstrated that \mathbf{D}_c (or $\mathbf{D}_{g,c}$) can be highly asymmetric. These results bring the notion of modelling the transport of active Brownian particles as normal advection and diffusion into question. In §6.2, we have briefly discussed how these dispersion tensors arise from the particles' motility. Since their physical origin is dispersion rather than diffusion, they do not necessarily conform to the symmetric and positive definite requirement of a diffusivity. This conclusion may have far-reaching consequences on how we interpret the dispersion of biological micro-swimmers such as algae in the wider context, such as the turbulent ocean. However, we have yet to discuss the physical implication of the asymmetric dispersion tensors \mathbf{D}_c and $\mathbf{D}_{g,c}$ and how they compare with \mathbf{D}_{GTD} in higher dimensions. Understanding the physical implications of \mathbf{D}_c and $\mathbf{D}_{g,c}$ in relation to the individual level dynamics remains the current subject of our work.

As pointed out by a recent review (Bees 2020), there is a gap between complex models of individual particles and their equivalent modelling at the continuum level. In particular, the restriction on the type of flow field imposed by the generalised Taylor dispersion model needs to be overcome to improve our understanding of many transport phenomena of ABP suspension. The presented method to model ABP transport without any restriction on the type of flow field is perhaps the most important consequence of this work especially from a practical perspective. In our numerical examples, we can also see that the presented method is at least as accurate as the GTD model, if not significantly better in some cases. Therefore, this work presents a

significantly improved model of ABPs transport in a dilute suspension. While the presented examples focused mainly on gyrotactic ABPs, the framework presented can also be extended to other types of taxes, such as phototaxis and chemotaxis, as well as other types of particle motions, such as the orientation-dependent sedimentation of elongated particles (e.g. Ardekani *et al.* 2017; Clifton *et al.* 2018; Lovecchio *et al.* 2019). Hence, the potential application of the framework presented in this work is vast.

However, the current framework needs further developments and analysis. In particular, a good model for the boundary condition for ABPs suspension is needed. For example, Ezhilan & Saintillan (2015) have demonstrated the important role of translational diffusion D_T in the wall accumulation near a no-flux boundary, which this work has yet to demonstrate. On the other hand, the microscopic interactions between the wall and individual ABPs remains a subject of future work. Even with the knowledge of microscopic interactions between the particles and the wall, translating the interactions into suitable boundary conditions at the continuum level remains an important challenge. To this end, the recent work by Chen & Thiffeault (2020) offers some insight into how one can account for the non-trivial and shape-dependent steric interaction with the wall.

Supplementary data. Supplementary movies are available online.

Funding. This work is funded by the President's PhD Scholarship of Imperial College London.

Declaration of interests. The authors report no conflict of interest.

Author ORCID. L. Fung, <https://orcid.org/0000-0002-1775-5093>;
Y. Hwang, <https://orcid.org/0000-0001-8814-0822>

Author contributions. R.B. had the original idea of the transformation technique under an asymptotic approximation. L.F. and Y.H. developed the theory and L.F. performed the simulations. All authors contributed to reaching conclusions and in writing the paper.

Appendix A. Derivation of the local approximation

Following the expansion of $\Psi = \Psi^{(0)} + \epsilon\Psi^{(1)} + \epsilon^2\Psi^{(2)} + \dots$ in §4.1, we substitute the expansion into the Smoluchowski equation (2.4) and yield the following set of equations at successive orders of ϵ :

$$\mathcal{O}(1) : \partial_T \Psi^{(0)} + \mathcal{L}_p \Psi^{(0)} = 0; \quad (\text{A } 1a)$$

$$\mathcal{O}(\epsilon) : \partial_T \Psi^{(0)} + \mathbf{p} \cdot \nabla_{\mathbf{x}} \Psi^{(0)} + \tilde{P}e_f \mathbf{u} \cdot \nabla_{\mathbf{x}} \Psi^{(0)} + \partial_T \Psi^{(1)} + \mathcal{L}_p \Psi^{(1)} = \tilde{D}_T \nabla_{\mathbf{x}}^2 \Psi^{(0)}; \quad (\text{A } 1b)$$

$$\mathcal{O}(\epsilon^2) : \partial_T \Psi^{(1)} + \mathbf{p} \cdot \nabla_{\mathbf{x}} \Psi^{(1)} + \tilde{P}e_f \mathbf{u} \cdot \nabla_{\mathbf{x}} \Psi^{(1)} + \partial_T \Psi^{(2)} + \mathcal{L}_p \Psi^{(2)} = \tilde{D}_T \nabla_{\mathbf{x}}^2 \Psi^{(1)}; \text{etc.} \quad (\text{A } 1c)$$

Integrating over \mathbf{p} -space, (A 1) becomes:

$$\mathcal{O}(1) : \partial_T n^{(0)} = 0; \quad (\text{A } 2a)$$

$$\mathcal{O}(\epsilon) : \partial_T n^{(0)} + \partial_T n^{(1)} + \nabla_{\mathbf{x}} \cdot \left[(\tilde{P}e_f \mathbf{u} + \langle \mathbf{p} \rangle^{(0)}) n^{(0)} \right] = \tilde{D}_T \nabla_{\mathbf{x}}^2 n^{(0)}; \quad (\text{A } 2b)$$

$$\mathcal{O}(\epsilon^2) : \partial_T n^{(1)} + \partial_T n^{(2)} + \nabla_{\mathbf{x}} \cdot \left[(\tilde{P}e_f \mathbf{u} + \langle \mathbf{p} \rangle^{(1)}) n^{(1)} \right] = \tilde{D}_T \nabla_{\mathbf{x}}^2 n^{(1)}; \text{etc..} \quad (\text{A } 2c)$$

At the transient time $t \gtrsim \mathcal{O}(1)$ and each order of ϵ , we assume the time dependency of $\Psi^{(i)}$ in \mathbf{p} -space has reached quasi-equilibrium, while the time dependency of $\Psi^{(i)}$ in \mathbf{x} -space is slow. In other words, we assume that, at each order, $f^{(i)}$ is independent of τ as it has reached quasi-equilibrium and $n^{(i)}$ independent of τ because it only varies at the slow time scale T . Therefore, equation (A 1a) now becomes

$$\mathcal{L}_p f^{(0)} = 0, \quad (\text{A } 3)$$

which implies that the leading order orientational distribution $f^{(0)}$ takes the homogeneous solution of $\mathcal{L}_p(\mathbf{x}, t)$ as the solution, i.e. $f^{(0)} = g(\mathbf{x}, T; \mathbf{p})$. Meanwhile, we multiply (A 2b) by $f^{(0)}$ and subtract it from (A 1b). This operation equivalent to the steps towards (3.3) in §3. The operation yields

$$\begin{aligned} & n^{(0)} \partial_T f^{(0)} \\ & + (\tilde{P}e_f \mathbf{u} \cdot \nabla_{\mathbf{x}} f^{(0)} - \tilde{D}_T \nabla_x^2 f^{(0)}) n^{(0)} - 2D_T (\nabla_{\mathbf{x}} f^{(0)}) \cdot (\nabla_{\mathbf{x}} n^{(0)}) \\ & + (\mathbf{p} - \langle \mathbf{p} \rangle^{(0)}) f^{(0)} \cdot \nabla_{\mathbf{x}} n^{(0)} + n^{(0)} (\mathbf{p} \cdot \nabla_{\mathbf{x}} f^{(0)} - f^{(0)} \nabla_{\mathbf{x}} \cdot \langle \mathbf{p} \rangle^{(0)}) \\ & + n^{(1)} \mathcal{L}_p f^{(1)} = 0. \end{aligned} \quad (\text{A 4})$$

Now, (A 4) can be rewritten as

$$[\mathcal{L}_p(\mathbf{b}_{g,D_T} + \mathbf{b}_{g,c})] \cdot \nabla_{\mathbf{x}} n^{(0)} + n^{(0)} \mathcal{L}_p [f_{g,u} + f_{g,D_T} + f_{g,c} + f_{g,\partial T}] + n^{(1)} \mathcal{L}_p f^{(1)} = 0, \quad (\text{A 5})$$

where $f_{g,\star}$ and $\mathbf{b}_{g,\star}$ are defined by (4.2). Equations (4.2) and (A 5) are the equivalent of (3.4) and (3.5) respectively. We can then follow the same derivation as §3, which would lead to

$$\begin{aligned} & \partial_T n^{(1)} + \nabla_{\mathbf{x}} \cdot \left[(\langle \mathbf{p} \rangle_g + \tilde{P}e_f \mathbf{u}) n^{(1)} \right] \\ & = \tilde{D}_T \nabla_x^2 n^{(1)} + \nabla_{\mathbf{x}} \cdot \left[(\mathbf{D}_{g,c} + \mathbf{D}_{g,D_T}) \nabla_{\mathbf{x}} n^{(0)} + (\mathbf{V}_{g,u} + \mathbf{V}_{g,D_T} + \mathbf{V}_{g,c} + \mathbf{V}_{g,\partial T}) n^{(0)} \right], \end{aligned} \quad (\text{A 6})$$

where $\mathbf{V}_{g,\star}$ and $\mathbf{D}_{g,\star}$ are defined according to (3.9-3.10).

Now, equation (A 6) is at $\mathcal{O}(\epsilon^2)$. If we are to recover how n evolve over the long time T , we can recompose $\partial_T n = \partial_T n^{(0)} + \epsilon \partial_T n^{(1)} + \dots$, by summing up (A 2a-A 2c) with the corresponding ϵ scaling while substituting (A 2c) with (A 6). Hence,

$$\begin{aligned} & Pe_s \partial_T n + \nabla_{\mathbf{x}} \cdot [(Pe_s \langle \mathbf{p} \rangle_g + Pe_f \mathbf{u}) n] \\ & \approx D_T \nabla_x^2 n + Pe_s^2 \nabla_{\mathbf{x}} \cdot \left[(\mathbf{D}_{g,c} + \mathbf{D}_{g,D_T}) \nabla_{\mathbf{x}} n^{(0)} + (\mathbf{V}_{g,u} + \mathbf{V}_{g,D_T} + \mathbf{V}_{g,c} + \mathbf{V}_{g,\partial T}) n^{(0)} \right]. \end{aligned} \quad (\text{A 7})$$

Note that we have only included $n^{(0)}$ and $n^{(1)}$ when recomposing n in this example as we are closing the problem at $\mathcal{O}(\epsilon^2)$. Therefore, (A 7) is accurate up to $\mathcal{O}(\epsilon^2)$. However, if we close the problem at a higher order, we can repeat a similar process from (A 4) to (A 6) at a higher order.

Here, we would argue that at the transient time $\tau \rightarrow \infty$, $\partial_t \approx Pe_s \partial_T$ and $n \approx n^{(0)}$. Because (A 7) is accurate up to $\mathcal{O}(\epsilon^2)$ while replacing $Pe_s^2 n^{(0)}$ with $Pe_s^2 n$ would only introduce an error at $\mathcal{O}(\epsilon^3)$, the substitution of $n^{(0)}$ by n shall not impact the accuracy of (A 7) tremendously. Under these approximations, we recover the approximated equation (4.1).

Appendix B. Analytical solution to a suspension of spherical gyrotactic active particles in a vertical flow

If the gyrotactic active particles in a vertical flow is spherical, the steady solution of (2.4) can be written analytically as $\Psi(\mathbf{x}, \mathbf{p}, \infty) = n_s(x) f_s(\mathbf{p})$, where

$$f_s(\mathbf{p}) = \frac{\beta}{4\pi \sinh \beta} \exp(\beta \cos \theta), \quad (\text{B 1a})$$

and

$$n_s(x) = A \exp\left(-\frac{\beta Pe_f W(x)}{2Pe_s}\right), \quad (\text{B 1b})$$

where A is the normalisation factor determined by the integral condition $\int_{-1}^1 n(x) dx = 1$. Equation (B 1) may also explain the results of Jiang & Chen (2020), who showed that the particle distribution is strongly dependent on β and the ratio between the two Péclet numbers (Pe_f/Pe_s).

If we substitute the corresponding parameters of this example into (3.8-3.11), we can recover

$$Pe_s D_{xx,c} \partial_x n_s = n_s \langle p_x \rangle_g, \quad (\text{B } 2)$$

which represents the equilibrium between a dispersion flux and the net-drift that is responsible for gyrotactic focusing. Note that $V_{x,c} = 0$ in this example because f_s is independent of \mathbf{x} . Here, to recover $D_{xx,c}$, we can substitute $f_s(\mathbf{p})$ into (3.4d) to get

$$b_{x,c}(\mathbf{x}; \mathbf{p}) = -\frac{Pe_s}{\beta S(x)} (f_s(\mathbf{p}) - g(\mathbf{p})), \quad (\text{B } 3)$$

and therefore

$$\begin{aligned} D_{xx,c} &= -\frac{Pe_s}{\beta S(x)} \left(\int_{S_p} f_s(\mathbf{p}) p_x d^2 \mathbf{p} - \int_{S_p} g(\mathbf{p}) p_x d^2 \mathbf{p} \right) \\ &= \frac{Pe_s}{\beta S(x)} \langle p_x \rangle_g. \end{aligned} \quad (\text{B } 4)$$

REFERENCES

ALT, W. 1980 Biased random walk models for chemotaxis and related diffusion approximations. *J. Math. Biol.* **9** (2), 147–177.

ARDEKANI, M. N., SARDINA, G., BRANDT, L., KARP-BOSS, L., BEARON, R. N. & VARIANO, E. A. 2017 Sedimentation of inertia-less prolate spheroids in homogenous isotropic turbulence with application to non-motile phytoplankton. *J. Fluid Mech.* **831**, 655–674.

ARIS, R. & TAYLOR, G. I. 1956 On the dispersion of a solute in a fluid flowing through a tube. *Proc. R. Soc. Lond. A* **235** (1200), 67–77.

BATCHELOR, G. K. 1970 The stress system in a suspension of free-force particles. *J. Fluid Mech.* **41**, 545–570.

BEARON, R. N. 2003 An extension of generalized Taylor dispersion in unbounded homogeneous shear flows to run-and-tumble chemotactic bacteria. *Phys. Fluids* **15** (6), 1552.

BEARON, R. N. & HAZEL, A. L. 2015 The trapping in high-shear regions of slender bacteria undergoing chemotaxis in a channel. *J. Fluid Mech.* **771**, R3.

BEARON, R. N., HAZEL, A. L. & THORN, G. J. 2011 The spatial distribution of gyrotactic swimming micro-organisms in laminar flow fields. *J. Fluid Mech.* **680**, 602–635.

BEES, M. A. 2020 Advances in Bioconvection. *Annu. Rev. Fluid Mech.* **52** (1), 449–476.

BRADY, J. F. & BOSSIS, G. 1988 Stokesian Dynamics. *Annu. Rev. Fluid Mech.* **20** (1), 111–157.

BRADY, J. F. & MORRIS, J. F. 1997 Microstructure of strongly sheared suspensions and its impact on rheology and diffusion. *J. Fluid Mech.* **348**, 103–139.

BRENNER, H. 1980 General Theory of Taylor Dispersion Phenomena. *PCH Physicochem. Hydron.* **1** (2-3), 91–123.

BRETHERTON, F. P. 1962 The motion of rigid particles in a shear flow at low Reynolds number. *J. Fluid Mech.* **14** (2), 284–304.

CHEN, H. & THIFFEAULT, J.-L. 2020 Shape matters: A Brownian microswimmer in a channel , arXiv: 2006.07714.

CHEN, S. B. & JIANG, L. 1999 Orientation distribution in a dilute suspension of fibers subject to simple shear flow. *Phys. Fluids* **11** (10), 2878–2890.

CLEMENT, E., LINDNER, A., DOUARCHE, C. & AURADOU, H. 2016 Bacterial suspensions under flow. *Eur. Phys. J. Spec. Top.* **225**, 2389–2406.

CLIFTON, W., BEARON, R. N. & BEES, M. A. 2018 Enhanced sedimentation of elongated plankton in simple flows. *IMA J. Appl. Math.* **83** (4), 743–766.

CROZE, O. A., ASHRAF, E. E. & BEES, M. A. 2010 Sheared bioconvection in a horizontal tube. *Phys. Biol.* **7** (4).

CROZE, O. A., BEARON, R. N. & BEES, M. A. 2017 Gyrotactic swimmer dispersion in pipe flow: Testing the theory. *J. Fluid Mech.* **816**, 481–506.

CROZE, O. A., SARDINA, G., AHMED, M., BEES, M. A. & BRANDT, L. 2013 Dispersion of swimming algae in

laminar and turbulent channel flows: Consequences for photobioreactors. *J. R. Soc. Interface* **10** (81), 20121041.

CUSSLER, EDWARD LANSING 2009 Dispersion. In *Diffusion: Mass Transfer in Fluid Systems*, 3rd edn., pp. 95–110. Cambridge University Press.

DELMOTTE, B., KEAVENY, E. E., PLOURABOUÉ, F. & CLIMENT, E. 2015 Large-scale simulation of steady and time-dependent active suspensions with the force-coupling method. *J. Comput. Phys.* **302**, 524–547.

DOI, M & EDWARDS, S.F. 1988 Brownian Motion. In *The Theory of Polymer Dynamics*, pp. 46–90. Oxford University Press.

DOMBROWSKI, C., CISNEROS, L., CHATKAEW, S., GOLDSTEIN, R. E. & KESSLER, J. O. 2004 Self-concentration and large-scale coherence in bacterial dynamics. *Phys. Rev. Lett.* **93** (9), 2–5.

DRESCHER, K., GOLDSTEIN, R. E. & TUVAL, I. 2010 Fidelity of adaptive phototaxis. *Proc. Natl Acad. Sci. USA* **107** (25), 11171–11176.

DUNKEL, J., HEIDENREICH, S., DRESCHER, K., WENSINK, H. H., BÄR, M. & GOLDSTEIN, R. E. 2013 Fluid Dynamics of Bacterial Turbulence. *Phys. Rev. Lett.* **110** (22), 228102.

DURHAM, W. M., CLIMENT, E., BARRY, M., DE LILLO, F., BOFFETTA, G., CENCINI, M. & STOCKER, R. 2013 Turbulence drives microscale patches of motile phytoplankton. *Nat. Commun.* **4**, 1–7.

DURHAM, W. M., KESSLER, J. O. & STOCKER, R. 2009 Disruption of vertical motility by shear triggers formation of thin phytoplankton layers. *Science* **323** (5917), 1067–1070.

ELGETI, J., WINKLER, R. G. & GOMPPER, G. 2015 Physics of microswimmers—single particle motion and collective behavior: A review. *Rep. Prog. Phys.* **78** (5), 056601.

EZHILAN, B. & SANTILLAN, D. 2015 Transport of a dilute active suspension in pressure-driven channel flow. *J. Fluid Mech.* **777**, 482–522.

FRANKEL, I. & BRENNER, H. 1989 On the foundations of generalized Taylor dispersion theory. *J. Fluid Mech.* **204**, 97–119.

FRANKEL, I. & BRENNER, H. 1991 Generalized Taylor dispersion phenomena in unbounded homogeneous shear flows. *J. Fluid Mech.* **230**, 147–181.

FRANKEL, I. & BRENNER, H. 1993 Taylor dispersion of orientable brownian particles in unbounded homogeneous shear flows. *J. Fluid Mech.* **255**, 129–156.

FUNG, L., BEARON, R. N & HWANG, Y. 2020 Bifurcation and stability of downflowing gyrotactic micro-organism suspensions in a vertical pipe. *J. Fluid Mech.* **902**, A26.

HILL, N. A. & BEES, M. A. 2002 Taylor dispersion of gyrotactic swimming micro-organisms in a linear flow. *Phys. Fluids* **14** (8), 2598–2605.

HINCH, E. J. & LEAL, L. G. 1972a The effect of Brownian motion on the rheological properties of a suspensions of non-spherical particles. *J. Fluid Mech.* **52** (4), 683–712.

HINCH, E. J. & LEAL, L. G. 1972b Note on the rheology of a dilute suspension of dipolar spheres with weak Brownian couples. *J. Fluid Mech.* **56** (4), 803–813.

HWANG, Y. & PEDLEY, T. J. 2014a Bioconvection under uniform shear: Linear stability analysis. *J. Fluid Mech.* **738**, 522–562.

HWANG, Y. & PEDLEY, T. J. 2014b Stability of downflowing gyrotactic microorganism suspensions in a two-dimensional vertical channel. *J. Fluid Mech.* **749**, 750–777.

ISHIKAWA, T., LOCSEI, J. T. & PEDLEY, T. J. 2008 Development of coherent structures in concentrated suspensions of swimming model micro-organisms. *J. Fluid Mech.* **615**, 401–431.

JEFFERY, G. B. 1922 The motion of ellipsoidal particles immersed in a viscous fluid. *Proc. R. Soc. A Math. Phys. Eng. Sci.* **102**, 161–179.

JIANG, W. & CHEN, G. 2020 Dispersion of gyrotactic micro-organisms in pipe flows. *J. Fluid Mech.* **889**, A18.

KESSLER, J. O. 1986 Individual and collective fluid dynamics of swimming cells. *J. Fluid Mech.* **173**, 191–205.

KOCH, D. L. & SUBRAMANIAN, G. 2011 Collective Hydrodynamics of Swimming Microorganisms: Living Fluids. *Annu. Rev. Fluid Mech.* **43** (1), 637–659.

LOVECCHIO, S., CLIMENT, E., STOCKER, R. & DURHAM, W. M. 2019 Chain formation can enhance the vertical migration of phytoplankton through turbulence. *Sci. Adv.* **5** (10), eaaw7879.

LUSHI, E., WIOLAND, H. & GOLDSTEIN, R. E. 2014 Fluid flows created by swimming bacteria drive self-organization in confined suspensions. *Proc. Natl Acad. Sci. USA* **111** (27), 9733–9738.

MANELA, A. & FRANKEL, I. 2003 Generalized Taylor dispersion in suspensions of gyrotactic swimming micro-organisms. *J. Fluid Mech.* **490**, 99–127.

NOTT, P. R. & BRADY, J. F. 1994 Pressure-driven flow of suspensions: Simulation and theory. *J. Fluid Mech.* **275**, 157–199.

PEDLEY, T. J. 2010 Instability of uniform micro-organism suspensions revisited. *J. Fluid Mech.* **647**, 335–359.

PEDLEY, T. J. & KESSLER, J. O. 1990 A new continuum model for suspensions of gyrotactic micro-organisms. *J. Fluid Mech.* **212**, 155–182.

PEDLEY, T. J. & KESSLER, J. O. 1992 Hydrodynamic Phenomena In Suspensions Of Swimming Microorganisms. *Annu. Rev. Fluid Mech.* **24** (1), 313–358.

SAINTILLAN, D. 2010 The Dilute Rheology of Swimming Suspensions: A Simple Kinetic Model. *Exp. Mech.* **50** (9), 1275–1281.

SAINTILLAN, D. 2018 Rheology of Active Fluids. *Annu. Rev. Fluid Mech.* **50** (1), 563–592.

SAINTILLAN, D. & SHELLEY, M. J. 2007 Orientational order and instabilities in suspensions of self-locomoting rods. *Phys. Rev. Lett.* **99** (5), 1–4.

SAINTILLAN, D. & SHELLEY, M. J. 2008 Instabilities and pattern formation in active particle suspensions: Kinetic theory and continuum simulations. *Phys. Rev. Lett.* **100** (17), 178103.

SAINTILLAN, D. & SHELLEY, M. J. 2015 Theory of Active Suspensions. In *Complex Fluids in Biological Systems*, pp. 319–355. New York: Springer.

SCHOELLER, S. F. & KEAVENY, E. E. 2018 From flagellar undulations to collective motion: Predicting the dynamics of sperm suspensions. *J. R. Soc. Interface* **15** (140), 20170834.

SIEROU, A. & BRADY, J. F. 2001 Accelerated Stokesian Dynamics simulations. *J. Fluid Mech.* **448**, 115–146.

SŁOMKA, J. & DUNKEL, J. 2017 Spontaneous mirror-symmetry breaking induces inverse energy cascade in 3d active fluids. *Proc. Natl Acad. Sci. USA* **114** (9), 2119–2124.

SUBRAMANIAN, G. & KOCH, D. L. 2009 Critical bacterial concentration for the onset of collective swimming. *J. Fluid Mech.* **632**, 359–400.

TAYLOR, G. I 1953 Dispersion of soluble matter in solvent flowing slowly through a tube. *Proc. R. Soc. Lond. A* **219** (1137), 186–203.

TORNBERG, A.-K. & SHELLEY, M. J 2004 Simulating the dynamics and interactions of flexible fibers in Stokes flows. *Journal of Computational Physics* **196** (1), 8–40.

TOWNSEND, ALEX, WILBER, HEATHER & WRIGHT, GRADY B. 2016 Computing with Functions in Spherical and Polar Geometries I. The Sphere. *SIAM J. Sci. Comput.* **38** (4), C403–C425.

VENNAMNENI, L., NAMBIAR, S. & SUBRAMANIAN, G. 2020 Shear-induced migration of microswimmers in pressure-driven channel flow. *J. Fluid Mech.* **890**, A15.

VOTH, G. A. & SOLDATI, A. 2017 Anisotropic Particles in Turbulence. *Annu. Rev. Fluid Mech.* **49** (1), 249–276.

WAN, K. Y. & GOLDSTEIN, R. E. 2014 Rhythmicity, Recurrence, and Recovery of Flagellar Beating. *Phys. Rev. Lett.* **113** (23), 238103.

WENSINK, H. H., DUNKEL, J., HEIDENREICH, S., DRESCHER, K., GOLDSTEIN, R. E., LÖWEN, H. & YEOMANS, J. M. 2012 Meso-scale turbulence in living fluids. *Proc. Natl Acad. Sci. USA* **109** (36), 14308.

WILLIAMS, C. R. & BEES, M. A. 2011 Photo-gyrotactic bioconvection. *J. Fluid Mech.* **678**, 41–86.

WIOLAND, H., WOODHOUSE, F. G., DUNKEL, J., KESSLER, F. O. & GOLDSTEIN, R. E. 2013 Confinement Stabilizes a Bacterial Suspension into a Spiral Vortex. *Phys. Rev. Lett.* **110** (26), 268102.